U.S. Coast Guard Research and Development Center

1082 Shennecossett Road, Groton, CT 06340-6096

Report No. CG-D-11-00

Assessment of Satellite and Airborne Synthetic Aperture Radar for U.S. Coast Guard Search and Rescue Planning

Final Report
March 2000

Prepared for:

U.S. Department of Transportation
United States Coast Guard
Marine Safety and Environmental Protection (G-M)
Washington, DC 20593-0001

N O T I C E

This document is disseminated under the sponsorship of the Department of Transportation in the interest of information exchange. The United States Government assumes no liability for its contents or use thereof.

The United States Government does not endorse products or manufacturers. Trade or manufacturers' names appear herein solely because they are considered essential to the object of this report.

This report does not constitute a standard, specification, or regulation.

Marc B. Mandler, Ph.D.
Technical Director
United States Coast Guard
Research & Development Center
1082 Shennecossett Road
Groton, CT 06340-6096

Technical Report Documentation Page

1. Report No.	2. Government Accession Number	3. Recipient's Catalog No.
CG-D-11-00		

4. Title and Subtitle

Assessment of Satellite and Airborne Synthetic Aperture Radar for U.S. Coast Guard Search and Rescue Planning

5. Report Date
March 2000

6. Performing Organization Code
Project No. 1012.3.9

7. Author(s)
J.E. Dick-O'Donnell [1], P. Bogden and J. O'Donnell [2], J. Lyden, D. Lyzenga, D. Miller and C. Wackerman [3]

8. Performing Organization Report No.
R&DC-125-99

9. Performing Organization Name and Address

U.S. Coast Guard [1]
Research and Development Center
1082 Shennecossett Road
Groton, CT 06340-6096

University of Connecticut [2]
Avery Point, CT 06340

ERIM International, Inc. [3]
Ann Arbor, MI

10. Work Unit No. (TRAIS)

11. Contract or Grant No.
DTCG39-94-D-E56616

12. Sponsoring Organization Name and Address

U.S. Department of Transportation
United States Coast Guard
Operations (G-O)
Washington, DC 20593-0001

13. Type of Report & Period Covered
Final Report

14. Sponsoring Agency Code
Commandant (G-OPR)
U.S. Coast Guard Headquarters
Washington, DC 20593-0001

15. Supplementary Notes
The R&D Center's technical point of contact is Dr. Jennifer Dick O'Donnell, 860-441-2741 or jdick@rdc.uscg.mil.

16. Abstract (MAXIMUM 200 WORDS)

The USCG R&D Center performed a feasibility study of the use of satellite and airborne synthetic aperture radar data to support ocean search and rescue planning. Three field experiments were performed to assess the capability of synthetic aperture radar images of surface features associated with ocean currents to provide surface current estimates for search planners. Advanced Very High Resolution Radiometry (AVHRR) and Radarsat synthetic aperture radar images from Georges Bank were obtained. Three methods to estimate surface currents from synthetic aperture radar imagery were investigated. Attempts were made to correlate AVHRR thermal features with synthetic aperture radar signatures. A second field experiment was performed off the coast of Delaware, to evaluate the potential of interferograms generated from complex Radarsat synthetic aperture radar data using a technique analogous to dual antenna interferometry. A third experiment was performed in Long Island Sound. Sea surface current estimates derived from airborne interferometric synthetic aperture radar (INSAR) data were compared with Acoustic Doppler Current Profiler measurements and the trajectories of surface drifters.

17. Key Words	18. Distribution Statement
airborne, satellite, synthetic aperture radar, search and rescue, sea surface currents	This document is available to the U.S. public through the National Technical Information Service, Springfield, VA 22161

19. Security Class (This Report)	20. Security Class (This Page)	21. No of Pages	22. Price
UNCLASSIFIED	UNCLASSIFIED		

Form DOT F 1700.7 (8/72) Reproduction of form and completed page is authorized.

[BLANK]

Executive Summary

A critical ingredient to any search plan is knowledge of the surface currents in the search area. Unfortunately, available information on currents derived from models and historical data introduces significant errors into the search plan. Ideally, surface currents in any part of the ocean should be measured in real-time. Remote sensing, either by aircraft or satellite, provides the potential for such.

In the past, the R&D program evaluated the utility of Advanced Very High Resolution Radiometry (AVHRR) for surface current estimation. It was concluded that while AVHRR can estimate surface currents, its operational utility is limited by its inability to penetrate clouds, fog, smoke or haze.

In this research, we evaluated the utility of synthetic aperture radar to measure currents. Synthetic aperture radar has been shown by others to image surface features associated with ocean currents and is unaffected by cloud cover and light conditions. This research addressed whether these sensors can provide the surface currents needed by search planners.

Several approaches for extracting surface current information from synthetic aperture radar ocean imagery have been examined and demonstrated with differing levels of success. These methods are based on a variety of techniques. In all cases, a lack of surface truth data hindered efforts to validate the models.

The question of whether a single antenna Interferometric Synthetic Aperture Radar (INSAR) technique could provide current information was investigated. INSAR was shown to be infeasible. A discussion of what radar parameters determine sensitivity to surface currents is presented, along with concepts of how a single antenna non-synthetic aperture radar system could be used to support Coast Guard operations.

The results of an airborne INSAR data collection and analysis are also presented. The initial comparison with ground truth was very poor. Further processing and reanalysis of the data produced a significantly better agreement, but led to grave concerns over the reliability and operational accuracy of the INSAR data.

The ability to acquire, process, and interpret the data in near real-time is critical to the success of a rescue mission. Spaceborne systems are not well suited to this for several reasons. First, spaceborne systems are constrained to a particular orbit. Therefore, there is a delay, which is a function of the revisit cycle and the sensor swath, for the sensor to image the area of interest. Second, the time between acquisition of two sequential images of the same region is likely to be operationally unacceptable. Third, the amount of time between placing an image request and image acquisition is ill suited to the mission. Fourth, without a real-time link, image delivery can take hours to days. Alternative satellite methods for current determination were briefly evaluated and quickly concluded that the techniques considered held little promise.

At present, satellite synthetic aperture radar is not feasible for operational Coast Guard search planning. Immediate on-scene data cannot be obtained due to Radarsat's orbit, ordering requirements and data delivery delays. Sea surface current information cannot be reliably extracted from single antenna systems. Ocean monitoring is not an option because of the Coast Guard's enormous operating area and cost considerations.

Table of Contents

List of Figures

List of Tables

List of Acronyms

ADCP	Acoustic Doppler Current Profiler
AVHRR	Advanced Very High Resolution Radiometer
DCS	Data Collection System
HH	Horizontally polarized transmitted and received
INS	Inertial Navigation System
INSAR	Interferometric Synthetic Aperture Radar
ISARC	Improvements to Search and Rescue Capabilities
R&D	Research and Development
RERSS	Radarsat Emergency Response Subscription Service
VV	Vertically polarized transmitted and received

[BLANK]

1 Introduction

Search and rescue cases frequently occur in regions of the ocean where it is difficult to obtain real-time sea surface conditions over large areas at the high spatial resolution needed for search planning. Search planners need real-time environmental data to estimate where the distressed vessel will have drifted by the time rescuers can arrive on scene. Methods presently used for estimating search object drift include the use of climatological and dynamic models, drifting buoys, and local wind conditions. Satellite observations, however, make it possible to obtain ocean surface conditions in areas that are otherwise inaccessible. The US Coast Guard Research and Development (R&D) Center has been evaluating whether remotely sensed ocean imagery can be used in an operational setting to provide ocean surface current estimates to support search and rescue planning.

The feasibility of using changes in sea surface temperature derived from sequential Advanced Very High Resolution Radiometry (AVHRR) imagery to routinely estimate surface currents has been investigated (Dick O'Donnell, 1998). Although the impact of cloud cover will vary with geographical location and season, for search and rescue planning, the inability of IR sensors (such as AVHRR or color scanners) to penetrate clouds, fog, smoke, and haze severely limits the operational feasibility of using only AVHRR imagery (Dick O'Donnell, 1997). This topic was investigated through the Improvement of Search and Rescue Capabilities (ISARC) Project at the Coast Guard R&D Center in the early 1990s. Further details about AVHRR and Search and Rescue planning are discussed in Dick (1992; 1994), Dick O'Donnell and Robe (1996; 1997) and Dick O'Donnell (1996). Because of the shortcomings of AVHRR, it has been the use of microwave instruments (such as synthetic aperture radar) with their all-weather, day-night capability that has resulted in the greatest advances in satellite oceanography. Synthetic aperture radar has been shown to image surface features associated with ocean currents and is unaffected by cloud cover and light conditions, thus synthetic aperture radar would be able to provide day/night, all-weather coverage of the sea surface. This is a major advantage of synthetic aperture radar for Search and Rescue over IR sensors (such as AVHRR and color scanners). This led the R&D Center to assess the capability of synthetic aperture radar images of surface features associated with ocean currents to provide surface current estimates for search planners.

The purpose of this project, RADARSAT Satellite All-Weather Surface Features, was to assess the capability of using satellite and airborne synthetic aperture radar ocean imagery in an

operational setting to provide surface current information to search and rescue planners. For synthetic aperture radar (or any sensor, for that matter) to be used successfully in an operational Coast Guard environment, the data must be timely and reliable, and the processing and distribution must be automated. The data source or collection scheme must be applicable to the US Coast Guard's large operating area, yet the resolution must be at a sufficient scale to provide useful on-scene conditions for the search planners. These requirements are the primary considerations when determining the feasibility of using remotely sensed oceanographic data for Coast Guard search planning. If these criteria cannot be met, then the methods will not be practical for search planning. A secondary consideration for operational use is the cost of the data collection including developmental, implementation, maintenance and operational costs. Commercially available satellite and airborne synthetic aperture radar imagery were considered for their potential for providing cost effective information over large search areas.

This report presents a summary of the findings on the operational feasibility of using satellite and airborne synthetic aperture radar for search and rescue planning. Included is a description of synthetic aperture radar imaging of the ocean surface in Section 2. Section 3 discusses satellite and airborne interferometric synthetic aperture radar (INSAR) current measurements including a description of the airborne data collection that was performed and the results of that effort. Alternative methods for using synthetic aperture radar for estimating sea surface currents are presented in Section 4. The results of a literature search on using a multi-sensor approach to estimating surface currents are presented in Section 5. Conclusions and Recommendations are found in Sections 7 and 8.

The research effort was designed to resolve two major issues. The first issue is technological: does the technique work and how accurate is it? The second issue is operational: how practical is the technique?

2 Synthetic Aperture Radar Imaging of the Ocean Surface

2.1 Theoretical Background

Synthetic aperture radar is a mature technique used to generate radar images in which detail can be resolved. Synthetic aperture radars provide unique capabilities as an imaging tool. Because they provide their own illumination (the radar pulses), they can image at any time of day or night,

regardless of sun illumination. In addition, because the radar wavelengths are much longer than those of visible or infrared light, synthetic aperture radars can "see" through cloudy and dusty conditions that visible and infrared instruments cannot. When synthetic aperture radar images moving objects, the Doppler-shift causes the objects to be smeared and their position shifted in the radar image. This phenomenon is exploited when imaging ocean features to detect the magnitude and direction of the underlying currents.

Each pixel in the radar image represents the radar backscatter for that area on the ground: darker areas in the image represent low backscatter, brighter areas represent high backscatter. In general, the higher or brighter the backscatter on the image, the rougher the surface being imaged (see Figure 1). Flat surfaces that reflect little or no microwave energy back towards the radar will always appear dark in radar images. Surfaces inclined towards the radar will have a stronger backscatter than surfaces that slope away from the radar and will tend to appear brighter in a radar image. The amount of backscatter also depends on the radar wavelengths used, the size of the scatterers, the moisture content of the area being imaged, the polarization of the pulses, and the observation angle.

Ocean surface features are visible in microwave images through the change in the small scale features on the sea surface (capillary waves) caused by the large scale features such as internal waves, bathymetric features and current fronts. The dominant mechanism for radar scattering from the ocean is Bragg scattering off water waves having wavelengths similar to that of the incident radar signal (Wright, 1966; Valenzuela, 1978). Radar signal wavelengths are typically between 1 cm (K-band) and 30 cm (L-band). Thus, the synthetic aperture radar signature of the ocean is proportional to the amplitude of specific capillary-gravity waves; short waves satisfying this resonance condition are referred to as Bragg waves. The modulation of the capillary-gravity waves by the underlying long waves has a significant impact on the radar cross-section (RCS) of the ocean. The longer-wavelength waves act upon the capillary waves through two important processes. First, these waves physically tilt the capillary waves riding upon them, altering the geometry of the scattering surface. This changes the ocean surface wave that is resonant with the sensor wavelength. Since this "new" Bragg wave will generally have a different amplitude than the original Bragg wave, the RCS will change (Wright, 1968; Plant, 1986). Second, orbital velocities associated with the long waves interact hydrodynamically with the capillary waves generally causing their amplitudes to increase near the crests of the long waves and to decrease

near the troughs. This RCS modulation makes it possible to detect long waves in synthetic aperture radar ocean imagery (Plant, 1986).

The presence of surface currents can also significantly affect synthetic aperture radar ocean imagery. As ocean waves enter regions containing surface current variations, wave-current interactions cause changes in the length, direction, and amplitude of the waves. By changing the amplitude and wavelength of the centimeter wavelength surface waves that are resonant with the synthetic aperture radar electromagnetic wavelength, surface currents can significantly change the RCS of the ocean surface (Lyzenga, 1991). Therefore, synthetic aperture radar ocean imagery may contain information regarding how both the Bragg waves and the long waves are influenced by the surface currents. It may be possible to use this information, in combination with wave-current interaction theory, to extract the underlying surface current gradients from synthetic aperture radar measurements.

Finally, surface currents may also be detected because they advect the ocean surface. Any waves or other features riding upon a surface current are advected by its underlying motion. It is sometimes possible to track distributed features, such as patches of surfactants or sea ice, with temporally sequential synthetic aperture radar images. By comparing sequential images, the movement of the features can be detected from which the speed and direction of surface currents can be inferred.

2.2 Field Tests

To evaluate the feasibility of synthetic aperture radar to estimate sea surface currents, a field experiment was performed on Georges Bank in June 1996 to obtain Radarsat data contemporaneously with AVHRR data and *in situ* measurements.

Three Radarsat synthetic aperture radar images collected over Georges Bank on 2 June (Figure 1), on 3 June (Figure 2), and on 13 June (Figure 3) were used in this study (see Table 1.). These images exhibit marked differences. The image on 3 June was collected in a different beam mode than the other two and shows none of the same detailed features. It is possible that some problem with this mode causes significantly more noise effects than in the other two. The general differences between the 2 June and 13 June images can be explained by the change in wind speed during the two collections. On 2 June the wind speed was

approximately 2.8 m/s, which is very low, and thus not much background clutter was generated on the ocean surface. This causes the dark regions in the upper portions of the image. In addition, the low wind allowed surfactants to gather at the surface, causing the dark, thin lines in the bottom portion of the image. On 13 June the wind speed had increased to approximately 4.3 m/s. This increased the background clutter, which generally raised the overall brightness of the image. In addition, the increased wind speed mixed the very near surface layer of the ocean thereby removing the surfactant streaks. Both the 2 June and 13 June measurements show marked differences between the upper left and lower right portions of the images. This represents a move from the continental shelf (upper left where bathymetry features can be seen mirrored in the synthetic aperture radar image) to deeper water (lower right where surface waves and internal wave features can be seen in the 13 June image). The 13 June image was selected for use in these studies because it had a much higher signal to background ratio than the 2 June image. Due to low wind speed conditions on 2 June, the amount of backscatter received from the ocean surface was too low to be measurable by the Radarsat synthetic aperture radar. The wind conditions at the time of the 13 June image were sufficient to provide enough backscatter to be useful in these analyses.

NOAA buoys (nos. 44011 and 44005) reported wind speed and direction data but current data was unavailable. Eleven self-locating drifting buoys were air-deployed on 1 June. By 13 June, the seven buoys still transmitting good position data had been transported to the southwest, beyond the area imaged by the Radarsat synthetic aperture radar. This lack of data is significant, as there was no surface truth data against which to compare the results. The possibility of improving observations of sea surface features by combining synthetic aperture radar and IR images obtained close in time was also of interest; however, no cross-sensor comparisons could be made, as all AVHRR data collected on 13 June was cloud filled over the area of the synthetic aperture radar image scene. This lack of surface truth hindered the validation of the model results.

2.3 *Estimating Sea Surface Currents from Synthetic Aperture Radar Imagery*

The capability of three methods to estimate surface currents from Radarsat synthetic aperture radar imagery for search planning was investigated. The first approach used an existing wave-current interaction model formulated by Lyzenga (1991) and applied by Johannessen et al. (1996) to estimate surface current gradients from changes in radar cross-section across synthetic aperture

radar signatures of bathymetric features. The wave-current model is used to compute the surface current gradients necessary to create the spatial dependence of the Bragg scattering observed in a given synthetic aperture radar image. These current gradients are then combined with local bathymetry and a simple flow model to compute the absolute current. Using the 13 June image, the RCS was estimated across the features in the upper left portion of the image (Figure 3). Figure 4 shows the results of this method when applied to the upper left portion of Figure 3.

The second method considered was the estimation of currents from wave refraction caused by underlying currents. Wave-current interaction theory is again used to develop a different model that computes surface currents from long wave (40 meters and longer) refraction evident in synthetic aperture radar ocean imagery. The dominant wavelength of the long waves and their direction of propagation at various positions can be estimated from the synthetic aperture radar image. If the dominant waves in each region of the image represent the same wave group, then wave-current interaction theory can be used to determine the surface current field necessary to produce the observed wave group variations (Figure 5). It was found, however, that changing the initial condition can have significant effect on the final current map (Figure 6). Therefore, an accurate initial current measurement is required.

The third method was to estimate current gradients from feature shifts, similar to feature tracking in IR imagery. By tracking distributed features (such as surfactants) visible in synthetic aperture radar ocean imagery, the speed and direction of the surface currents can be estimated by the motions of surface features using sequential synthetic aperture radar images. This method is only viable if trackable features are present in both images. Additionally, it may estimate only a projection of the current, rather than the total current magnitude.

2.4 Technical Evaluation

The capability of the methods considered to estimate sea surface currents is summarized below and discussed in greater detail in Miller et al. (1997) and Miller et al. (1999). Using a small-scale wave-current interaction model, it was demonstrated that it is possible to get current gradient information from relative changes in RCS over frontal and bathymetric features. Also, some information about the current direction and relative strength of the changes in the x and y components of velocity was derived from meandering features. Two issues were clear in analyzing the data. First, bathymetric data that is more accurate (specifically bottom slope) would

be needed to derive accurate absolute currents. Second, the model here gave current gradients that were most likely too high for reasonable ocean conditions. This overprediction is consistent with previous studies. More work is needed to establish a more precise model for C-band radars.

The second technique, inversion of long wave refraction patterns, shows some promise if a reasonable initial condition can be established. Without this, the variability of the estimated current fields due to inaccurate guesses of the initial currents is too great to be useful.

Feature tracking could not be evaluated from the field data due to a lack of trackable features and the time lag between the sequential Radarsat images. However, it is a direct method that works well under simple current conditions when distributed surface features are present in an image. The main obstacle to feature tracking is that the same feature must be present and identified in each of a time series of images.

2.5 Operational Evaluation

Under moderate wind speeds, the Radarsat imagery detected characteristics of the surface wave field, surface expressions of internal waves, and ocean surface features such as fronts, eddies, and surface films. For winds above 10-12 m/s, ocean features are no longer discernible because of surface mixing and the growth of wind waves (Johannessen et al., 1996). This restricts the use of feature tracking with synthetic aperture radar for search planning since wind speeds frequently exceed this limit during search and rescue missions.

The operational feasibility is also limited by the degree of user interaction required. Once the synthetic aperture radar images have been acquired, potential features need to be identified for analysis. All the non-interferometric procedures considered in this study require that some specific type of feature is visible in the imagery. Identification of these features requires personnel with synthetic aperture radar image interpretation skills. Classification of synthetic aperture radar ocean features is still an active area of research. Many factors can influence whether a region should be analyzed with a particular algorithm. Each of the three methods discussed has a straightforward mathematical foundation that can be implemented as part of a user-friendly software package. Assuming a skilled and experienced user with good synthetic aperture radar interpretation skills and a familiarity with the software package, the time required to acquire user input and process the data for each of these techniques is probably on the order of

half an hour to an hour. Interactive input from the user requires the greatest amount of time. The amount of user interaction required depends directly on the method being applied with the feature tracking method requiring the least.

Using long wave refraction to estimate the current field requires surface truth for initialization. This method is not based on synthetic aperture radar imaging theory, but rather on the hydrodynamic processes involving the propagation of long waves superimposed onto surface currents. Some drawbacks of this model are apparent. First, accurate spectral estimation places restrictions on the minimum size of the imagery subsets; however, the subsets must be small relative to the spatial scale of the surface current variations so changes can be resolved in the long waves as they propagate through the region. In addition, long wave modulation is not always detectable in synthetic aperture radar imagery, especially for low wind speed conditions. This method also assumes that the long waves are not influenced by the local winds, which may be incorrect under some conditions. Lastly, this method requires an accurate initial current measurement (from a moored or drifting buoy, for instance) to be useful.

Distributed feature tracking is only an option for airborne data. With the present satellite synthetic aperture radar systems, the time between successive images is too long for feature tracking. Regardless of the synthetic aperture radar system, this technique is constrained by the need for trackable features. Given the presence of distributed features in sequential images, implementation of this process is straightforward and will provide a simple current estimate. However, this method should not be considered a reliable technique since these features are often not present in synthetic aperture radar imagery.

3 Interferometric Synthetic Aperture Radar

Interferometric analysis of synthetic aperture radar imagery has received considerable attention recently [Goldstein and Zebker, 1987; Shemer *et al.*, 1993; Lyzenga and Malinas, 1996]. These methods typically rely upon two-antenna synthetic aperture radar systems, which consist of a pair of antennas separated by a distance D in the along-track (azimuth) direction. The basic concept behind the interferometric approach is given by Raney (1971). A coherent measurement of the target is made with the first antenna. After a slight time lag, an additional measurement of the target is made by the second antenna from the same location as the first measurement. If the coherence time of the target is longer than this time lag, then the phase difference between the

two measurements is equal to the product of the time lag and the radial component of the target's velocity. Thus, the radial component of the target velocity can be extracted directly from the phase difference of the two images.

Only one component of the scatterer velocity can be measured by an INSAR system. Therefore, it is necessary to fly the synthetic aperture radar platform in a multi-sided pattern around the region of interest to determine the two-dimensional velocity field. This is feasible for airborne systems, but poses a clear obstacle for spaceborne platforms. It is also important to note that the radar cannot distinguish between cross-track drift of the synthetic aperture radar platform and the radial motion of the ocean surface scatterers. Errors introduced by platform motion are typically removed by including a stationary target, such as land, in the imagery scene. In ocean regions where no stationary references are available, highly accurate knowledge of the synthetic aperture radar antenna position is necessary. This position information is typically provided by inertial navigation systems in conjunction with differential GPS.

3.1 Satellite INSAR

3.1.1 Background

One of the objectives of this study was to evaluate the potential of single antenna Synthetic Aperture Radar interferometry and furthermore, to evaluate the utility of this technique using six Radarsat scenes collected off the mouth of Delaware Bay in January 1998. Interferometry normally utilizes phase differences between two antennas or apertures to compute motion. Given the relatively long period of observation of synthetic aperture radar, it has been postulated by some that the antenna beam could be split to provide two independent observations of a scene from which phase differences, and hence motion, could be determined. If possible, a single antenna technique would allow current measurements to be performed from currently available satellite synthetic aperture radar systems such as Radarsat and ERS-1/2.

Below is a review of the theory behind single antenna interferometry. This is followed by a description of an alternative single antenna technique for deriving surface current information. An extension of this discussion describes ways to optimize a system for current measurements.

Following the work of Jensen and Chapman (1990), assume that the scattering surface consists of a single point scatterer. This scatterer has a position $r_s(t)$ that is given by

$$r_s(t) = r_0 + vt \tag{1}$$

where r_o is the initial position, v is the particle velocity and t is time. For this discussion, it is assumed that the scatterer is moving at a constant velocity. The radar has a position $r_r(t)$ that is given by

$$r_r(t) = r_1 + Vt \tag{2}$$

where r_1 is the initial position of the radar and V is the sensor velocity. The round-trip phase change from the radar to the scatterer and back to the radar is

$$\phi(t) = 2k\left|r_r(t) - r_s(t)\right| \tag{3}$$

which can be found by

$$\phi(t) = 2k\sqrt{\left|r_1 - r_0\right|^2 + 2(r_1 - r_0)\cdot(V - v)t + \left|V - v\right|^2 t^2} \tag{4}$$

Any phase shift caused by reflection has been neglected.

This phase function has only three degrees of freedom. These are the coefficients of *1*, *t*, and t^2 in the square root. Therefore, three measurements of the phase will determine the complete phase history. The information that results from knowing these coefficients can then be analyzed.

The constant term is

$$c_0 = \left|r_1 - r_0\right|^2 \tag{5}$$

This term represents the distance from the radar to the scatterer at time zero. It does not contain any scatterer velocity information.

The linear term is

$$c_1 = 2\left(r_1 \cdot V - \left(r_1 - r_0\right) \cdot v - r_0 \cdot V\right) \tag{6}$$

The first term is independent of the scatterer position or velocity. The second term represents the range component of the scatterer velocity. The third term represents the azimuth position of the scatterer. Knowing the value of c_1 does not allow separating out the effect of scatterer range velocity and azimuth position. For any given value of the range velocity of the scatterer, there is an azimuth position that results in the measured value of c_1. There is no determination of the range velocity from this function.

The quadratic term is

$$c_2 = \left|V - v\right|^2 \tag{7}$$

This term depends principally upon the azimuth velocity of the scatterer. For any given value of the range velocity of the scatterer, there is an azimuth velocity that results in the measured value of c_2. There is no determination of the range velocity from this function.

Therefore, three pulses from a single antenna define the entire phase history of a single point scatterer, and that history does not resolve an ambiguity between range velocity and azimuth position. Since a single antenna cannot determine the velocity of a single scatterer, it cannot determine the velocity of a set of scatterers within an image.

3.1.2 Technical Evaluation

A theoretical analysis of single antenna INSAR reveals that three pulses from a single antenna define the entire phase history of a single point scatterer, and that history does not resolve an ambiguity between range velocity and azimuth position. Since a single antenna cannot determine

the velocity of a single scatterer, it cannot determine the velocity of a set of scatterers within an image.

It is concluded that a single antenna technique cannot determine the velocity of a moving scatterer whose azimuth position is unknown. Two or more antennas are required to make such a measurement. Six Radarsat scenes were collected off the mouth of Delaware Bay in January 1998 to evaluated the potential of single antenna Synthetic Aperture Radar INSAR. However, based on this conclusion, it was decided not to pursue single antenna interferometry measurements from Radarsat imagery. An alternative technique for deriving current measurements using synthetic aperture radar data is discussed in Section 4.

3.2 Airborne INSAR

The INSAR approach has been applied to synthetic aperture radar ocean imaging with success.

3.2.1 Survey of Experimental Results

A number of studies have been completed to test the validity of using INSAR to measure ocean surface currents. Table 2 summarizes the date, system, and surface truth used for comparison.

Goldstein et al. (1989) monitored the location of Lagrangian drifters during two INSAR flights near San Diego, California. The drifters were constructed of thin pieces of plywood to make the drifter insensitive to wind and short wave motion and to maximize the influence of surface currents. Current estimates from the two sources were found to be linearly related (a slope of 1.12 ±0.18), with a bias of 2.2 cm/s and RMS error of 12 cm/s. They reported that the bulk of the error was due to three points; no reason for eliminating these points was given. Using the drifter velocity as the true surface current velocity, Goldstein et al. come to two main conclusions regarding the relationship between the INSAR and surface currents.

1. INSAR is most effective when looking along direction of strongest flow.
2. INSAR is most accurate when looking up or down wind. This is due to less ambiguity in the Bragg wave velocity contribution.

The first conclusion is simply a statement about the sensitivity of the INSAR measurement. Since the component of velocity toward the radar is all that is measured, as that component gets smaller, the associated variability in the measurement will increase. The second conclusion is due to the

inherent ambiguity when Bragg waves are moving toward and away from the sensor. If the ambiguity is eliminated, the measurement will be more accurate.

Thompson and Jensen (1993) compared INSAR derived and in situ measurements of current variations across internal wave features. The INSAR measured variations were approximately ten times those derived from in situ measurements (subsurface current meter measurements projected to the surface). A model was used to explain that this amplified modulation is due to changes in the Bragg wavelengths as they are advected by the longer swell or internal waves. The model suggests that the sensitivity of INSAR to Bragg wave velocity variations decreases with increasing wavelength.

Shemer et al. (1993) measured longshore current velocities in Monterey Bay, California with INSAR and compared these current with Langrangian drifter-derived currents. The drifters were similar to those used in (Goldstein, et al., 1989). Shemer et al. note that in most cases the discrepancy between INSAR and in situ measured currents does not exceed several cm/s.

The most comprehensive study published to date comparing INSAR data with surface measurements is from Graber et al. (1996). This study compared INSAR derived current measurements with HF Radar current measurements taken during the High-Resolution Remote Sensing Experiment (High-Res) off the coast of Cape Hatteras, North Carolina. When looking at a two-dimensional field, the rms error in magnitude and direction of measured current is 0.06 m/s and 14°, respectively.

3.2.2 Available INSAR Systems

An international survey (Kramer, 1996) reported five airborne synthetic aperture radar systems capable of along-track interferometry. Only these systems are represented in recent publications of airborne interferometric studies. Of these, three were built and are now operated by organizations in the USA, one is Canadian and the last is German. Details about the various interferometric airborne synthetic aperture radar systems are presented in Section 2.4 of Miller et al. (1999). Cost information on owning and operating an INSAR system can be found in Appendix A: Cost Pertaining to INSAR Systems.

3.2.3 Airborne Experiment

It was initially planned to evaluate the operational feasibility of using airborne INSAR during LOST 98, a comprehensive R&D Center data collection effort in January 1998. Due to mechanical problems in the aircraft, no airborne INSAR data was collected during the experiment.

A separate experiment therefore took place in late July on Long Island Sound. Since the current in the ocean can not be controlled, a test site was chosen at which the surface current distribution could be estimated by an established approach and a range of values could be observed. A region of complex bathymetry in central Long Island Sound, centered at approximately 41° 12′ North, and 72° 40′ West, was selected for the intercomparison experiment (see Figure 7). This site was selected because the current was known to vary from 0 to 50 cm/s in six hours due to the semi-diurnal tide height fluctuations at the eastern end of the Sound. Further, it was anticipated that the presence of Falkner's Island and the steeply sloping bottom would result in significant, instantaneous, spatial gradients as well.

Three alternative measurement techniques were considered: an array of moored current meters, drifting buoys, and ship-mounted acoustic Doppler current profiler (ADCP) observations. Since moored current meters have a small sample volume and coverage of a large area is expensive, this option was dismissed. The drifter option was also dismissed because of the difficulty in keeping them in the survey area during the survey period and maintaining spatial separation of the drifters. The remaining option was therefore adopted.

Ship mounted ADCP surveys have disadvantages in this application: estimates can only be obtained at approximately 1 m below the surface and the ship takes much longer to survey the test area than the aircraft. The ADCP option was nonetheless deemed the most appropriate because the circulation in the test area is mainly driven by the barotropic tide. Consequently, the currents are periodic in time and have little vertical gradient near the surface. This choice of site therefore mitigated the problem with differences between the surface current observed by the INSAR and that observed by the ADCP at 1m. The periodic nature of the circulation can also be exploited to mitigate the disparity in the survey times. Bodgen and O'Donnell (1998) have demonstrated that several days of current surveys can be extrapolated in time and space to yield accurate, instantaneous maps of the tidal currents that are consistent with the sea level observations, the geometry and bathymetry of the estuary, and linearized dynamics and kinematics.

In summary, the intercomparison presented is between the surface current in the test area estimated using the INSAR system and the current fields obtained by the generalized inverse analysis of ADCP surveys in the test area. Inverse analysis allows data to be used in a model to estimate parameters of the model. Inverse analysis of the ADCP data then provides objective interpolations in space and time. ADCP based estimates can then be compared to the nearly synoptic INSAR estimates of the current. Any differences between the two estimates were evaluated by estimating the contribution to the difference expected to result from near surface shear, errors in the ADCP measurements, and the uncertainties associated with the generalized inverse analysis. The technical details associated with the various techniques (INSAR observations, ADCP observations, and generalized inverse analysis) can be found in Bogden (1999) and O'Donnell (1999).

3.2.4 Interferometric Analysis

On August 1, 1998, the ERIM INSAR system was flown over the test area in Long Island Sound. The spatial resolution of the data was approximately 10 m. The swath width of the sensor was approximate'y one third of the width of the test area and therefore three passes were required to obtain the distribution of a single velocity component. This took approximately 20 minutes. Approximately 20 minutes later a further three passes in the orthogonal direction were executed.

Three overlapping north-south INSAR Data Collection System (DCS) passes were followed by three overlapping east-west passes. Each pass was 11.1 km in length with a recorded swath width (ground plane) of approximately 2.4 km. This collection pattern is depicted graphically in Figure 7. The INSAR can only determine line-of-sight current measurements and orthogonal measurements are needed to produce current vectors. A total of 26 passes were collected, including four sets of the three N-S and three E-W passes as well as a land pass at the beginning and again at the end of the flight to provide stationary scene data for calibration.

Following the data collection, the INSAR data set was processed and analyzed to provide surface current estimates. Efforts were concentrated solely on the vertically polarized (VV) data as it has inherently higher clutter-to-noise than the horizontally polarized (HH) and presumably will provide better estimates. The entire VV data set was processed into complex imagery. To increase efficiency, only the center 60 seconds (6km) or so from each pass was processed which included

the orthogonal data. An example VV image from one of the antennas is shown in Figure 8. This same six-pass sequence was repeated four times during the INSAR collection to provide data under changing tidal conditions.

Table 3 presents the times of the beginning and end of each survey and the velocity component observed. Note that there is a time delay between the estimates of the current components so that the velocity vector must be recognized as not being synoptic. Since the time scale for variations in the current field is approximately 12 hours, the 30 minute offset between the times of the east and north components should not be a large error.

The complex image from one antenna is multiplied by the complex conjugate of the other antenna to form the interferogram for this pair. The phase of the interferogram is corrected for system effects which are determined using the phase function derived for the land scenes which are stationary. These system-related effects are due to factors such as mounting errors of the antennas which produces a range-dependent phase function across the imaged scene that is unrelated to surface motion. This corrected phase can be directly converted into surface currents.

As an example, data from an E-W pass were used to generate a current map in the overlapped region. This set was chosen due to the presence of a few small islands that were exposed to varying degrees during the collection. The procedure outlined above was used along with low-pass filtering to produce a two-dimensional current estimate. These current estimates are depicted as vectors and are shown in Figure 9 overlaid on the image from the E-W pass. The length of the vector is scaled to the peak current magnitude (.92m/s) with direction indicated by the arrow. The currents are seen to be generally southerly with magnitudes averaging around .5m/s or 1kt. The smallest current magnitudes are observed over the islands; the magnitude of the current estimates over land provides a rough estimate of the noise in the measurements.

Following the same procedure, the currents were calculated for the same spatial coverage based on images collected approximately three hours later and therefore, under different tidal conditions. The result is shown in Figure 10. The image shows that the water level has risen as the islands (particularly the small island to the west) appear smaller. The currents are still in a generally southerly direction with slightly smaller magnitudes (peak value .69m/s) than earlier in the flight.

INSAR may accurately measure the velocity of the radar scatterer, however this is not the same as the ocean surface current. It is generally agreed that the radar only responds to small wavelength waves (see Valenzuela, 1978) known as Bragg waves. Assuming Bragg waves are the dominant scatterer for the ocean surface, then the scatterer velocity is given by the sum of three components. These are the actual surface current velocities (with any wind-driven components), the orbital velocity of the underlying long waves, and phase speed of the Bragg waves. Since the surface current is the only contributing velocity that is of USCG interest, the other components will need to be compensated for when estimating the surface current.

Wind driven currents magnitudes are typically on the order of 3% - 4% of the wind velocity measured at 10m (Banner and Phillips, 1974), so their contribution to the measured velocity may not be significant. To remove the component, it is necessary to have some measure of wind speed. If it can be assumed that the wind speed does not vary over the area of interest, a single measurement would be sufficient. Otherwise, an array of sensors or model output would be required.

If the resolution of the synthetic aperture radar image is coarse enough, the orbital velocities of the underlying long waves will average to zero. This happens because the orbital velocity is periodic, and velocities from the wave peak will cancel the velocities from the wave trough. Since the orbital velocity averages to zero, it is only necessary to make sure that the resolution of the current estimate is relatively coarse. Alternatively, if it is necessary to have a high-resolution current map, orbital velocities will appear as regular variations in the surface current estimate.

The most complicated factor in estimating the surface current is the Bragg wave velocity. As mentioned previously, the INSAR system responds only to the Bragg waves that appear on the ocean surface. For the DCS sensor at 45°, the Bragg wave has a velocity of approximately 0.19 m/s.

In general, the radar will "see" Bragg waves that are moving toward and away from the sensor. Each of these wave groups will contribute to the measured velocity. Note that since the wave groups are traveling in opposite directions that the velocities will tend to cancel each other to some extent, though not completely.

Some characteristics and weaknesses in the observations were immediately apparent. First, the north components of velocity are predominantly large (~0.4 m/s) and negative. Between 05:25 and 05:47, however, the north component of the flow is large (~0.4 m/s) and positive. These large magnitudes in the across-isobath direction are implausible. Secondly, there is evidence of discontinuities across the swath boundaries in the east components that are particularly strong. These are also implausible and indicate problems with the processing algorithm.

3.2.5 ADCP Observations

Observations of the vertical profile of the current in the experiment area were made from the RIV UConn with a RDI 1200kHz broad band acoustic Doppler current profiler mounted over the side of the vessel. The ADCP observations formed the input data to the inverse model. The track of the vessel during the survey period (July 29th -August 1st, 1998) is shown in Figure 11. This track was a compromise between covering the whole domain and getting a complete survey between three and four times every tidal cycle (approximately 12 hours). The circuit shown by the solid line in Figure 11 was completed six times in approximately eighteen hours and then a leg to the south east corner of the domain was added (indicated by the dashed line in Figure 11) to improve the analysis in that area. Seventeen loops were completed during the 61-hour survey. Two of these occurred while the DCS was airborne.

Figure 12 shows the ADCP observations at four periods in a 0.35m bin centered at 1.3 m below the surface. These are a small subset of the data used in the generalized inverse analysis to provide synoptic map of the velocity throughout the survey domain. Though the flow is varying in both space and time, these observations provide the general pattern of the tidal circulation during the INSAR over flight. The flow is mainly directed to the west early in the survey (see Figure 12a, at approximately 0.30 m/s. By the end of the survey the westward current has reduced to less that 0.1 m/s. In all the surveys a southward flow of approximately 0.2 m/s is apparent.

A preliminary evaluation of the performance of the INSAR was obtained by comparing the component magnitudes obtained from the INSAR survey with the ADCP derived vectors in Figure 12. This demonstrated some similarities and some major discrepancies in magnitude and direction.

Since the ADCP data is not available throughout the domain during the INSAR surveys, a more effective evaluation requires that the fields derived from the generalized inverse analysis of the full 61hour data set is compared with the INSAR estimates.

3.2.6 Generalized Inverse Analysis

To provide instantaneous fields of velocity from the 61 hours of current surveys by the R\V UConn, the method of Bogden and O'Donnell (1998) was employed. The technique allows the observations to be interpolated and extrapolated in space and time in a manner that is statistically consistent with linearized long wave dynamics, sea level variations at Montauk Point, NY, and the geometry of Long Island Sound. Complete details of the application of the method in this project are described in Bogden (1999). The resolution of the analysis was 0.57 km in the east direction and 0.75 km in the north direction. These choices are consistent with the resolution of the ADCP survey and are adequate to resolve the dominant features of the bathymetry of the survey area.

Maps of ocean-surface currents were produced for 1 August 1998. The maps are based on data collected from ship surveys with an ADCP. The analysis involved 3 major steps: (1) development of a computer model for tidal currents for all of Long Island Sound for the period of interest, (2) tide-removal from the observations using a generalized inverse analysis based on the tidal model, and (3) statistical mapping of the non-tidal surface currents. Very conservative upper bounds on the root-mean-square error in the resulting currents is 20.4 cm/s, most of which is due to unmeasured current shear between the sea surface and 1.3 meters depth.

Hourly maps of absolute surface currents were generated for the period from 0200 through 0700 EDT on 1 August 1998. The underlying fields (at half-hourly intervals) were analyzed and compared with independent measurement of surface currents.

At 0200 EDT, the current is uniformly westward at slightly less than 50 cm/s. In the vicinity of Falkner Island the flow veers northward, and locally the speed exceeds 50 cm/s. The pattern at 0300 EDT is still generally westward at around 50 cm/s, though there is somewhat more structure in the vicinity of Falkner Island. By 0600 EDT the flow to the north of Falkner Island is not significantly different from zero, and there is some weak flow toward the SE in the southern part

of the domain. At 0600 EDT the ebb has begun and there is eastward flow in the NW corner of the domain. Note that during the entire period, the currents rarely exceed 50 cm/s.

Tide-Removed Surface Currents

ADCP data is collected in "bins," that is, the current velocity is averaged over a certain depth range, a bin, which is a function of the total water depth. The "surface-shear" component is, by definition, the velocity of bin 2 (centered 1.3 meters below the surface) minus the best estimate of the depth-averaged tidal flow. The velocities represent depth-averaged ADCP measurements, before inversion, obtained by bin-averaging in time and space to one of 14 locations that was repeatedly sampled by the ship. The binning procedure produces a set of discrete independent data points with nearly homogeneous spatial sampling. The currents are dominated by tidal flow with amplitudes of 40-50 cm/s, and velocities are predominantly east-west. The tides were estimated with the generalized inverse model described in the next section. The surface-shear velocity defined this way is not sensitive to the choice of bin as long as the top-most bin is not used since it suffers from surface-noise effects.

It should be noted that the flow field at depths shallower than 1.3 meters may well differ by up to 100% of the values from the lower bins. Such flows are not measurable with the shipboard ADCP and, as discussed below, account for the largest source of error in estimating surface current. Nevertheless, the estimated surface-shear velocities are small relative to the tidal flows. Furthermore, during the 3-day measurement period large-amplitude velocity shear was rarely observed in the top-most ADCP bins. Therefore, any differences between the maps of absolute surface current presented here and analogous maps obtained by alternate measurement techniques should not exceed 20 cm/sec. In other words, the absolute surface-current maps presented should not differ substantially from unmeasured currents shallower than 1.3 meters depth. Thus, for the study region and time period of interest, surface currents are dominated by the depth-averaged tidal flow, which is predominantly east-west on spatial scales resolved by the data.

Generalized Inverse Analysis of Tidal Flow

The technical details of the generalized inverse analysis performed for this analysis are identical to those described by Bogden and O'Donnell (1998).

The model does well at modeling the gross tidal variability. This is consistent with findings of Bogden and O'Donnell (1998) for a region in western Long Island Sound. The difference between

the estimated data and the prior tidal model data shows that some "tide-like" variability remains in the residual, which indicates errors in the dynamics of the prior tidal model with rms magnitude exceeding 10 cm/s.

The generalized inverse analysis (Bogden and O'Donnell, 1998) is designed to improve the tidal model. The inverse solution is visually identical to the data. The inverse adjustments are in the range of 10 to 20 cm/s. These adjustments are comparable in size to those of the surface-shear velocity described above. The rms error in the tidal flow estimates from the generalized inverse is 4 cm/s. Thus, the inverse analysis is necessary if errors in surface current maps are to be reduced below 10 cm/s.

Reliability of the Surface-Current Maps

The residual model-inverse misfit represents bin-averaged data measured by the ship. The bin-averaging was designed such that each data point in the plot is independent of every other. The rms misfit for depth-averaged tidal flow is 4 cm/s. That is, the standard error for the inverse estimates of depth-averaged tidal flow is 4 cm/s.

Twenty cm/s is a conservative estimate for the standard error of the surface-shear velocity discussed above. It is not possible to accurately estimate the shear in the upper 1.3 meters of the water column during this period, since the ADCP measurements leave this shallow layer unmeasured. Therefore, 20 cm/s was used as a conservative upper bound on the rms unmeasured shear.

The standard error for the maps of absolute surface velocity, which is the sum of optimized tides and objectively analyzed surface-shear velocity, is 20.4 cm/s. This is a very conservative estimate of the error in the velocities. Any surface current measurement technique should produce maps that have an rms difference of 20.4 cm/s from the absolute surface current estimates.

3.2.7 Comparison of Analyzed ADCP and INSAR Fields

The INSAR velocity field estimates were averaged into bins the same size as the grid cells used in the generalized inverse analysis of the ADCP data. Comparison of the INSAR estimates with the analyzed fields suggests that the north components of the INSAR estimates are too large and the sign reversal between 04:22 and 05:25 is clearly an error.

The most unambiguous means of comparison is to plot the value the velocity components estimated by the two techniques. Perfect agreement would result in the data points clustering along a straight line with unit slope through the origin. Figure 13 shows a comparison of the east components estimated using INSAR plotted against the estimates from the analysis of the ADCP data at four different times and Figure 14 displays the north components in a corresponding manner. Though the precise times of the ADCP analyses and the INSAR survey are not exactly the same, the time discrepancies do not have significant effects on the velocity errors. The comparison is very poor.

Based on this analysis, ERIM International, who performed the airborne INSAR processing, regenerated surface current maps. The normalization process that was used initially was incorrect in that it introduced a gradient at the edges of the images. Additionally, the currents provided were not corrected for the phase speed of the Bragg waves or the wind drift. These have to be taken into account before comparing with ground truth. The recalculated INSAR currents are dominantly East-West currents with very little North-South components similar to the ADCP measurements and the generalized inverse analysis. However, ERIM still experienced difficulties in calibrating the passes that did not contain islands. This was attributed to a drift in the sensor during the collection that was not accounted for by the inertial navigation system (INS).

Based on the revised data: (1) The INSAR estimated N-S currents are all small and each group of three passes is consistent in that they are the same to within the error bars (no DCS drift effects are evident); (2) The E-W currents definitely suffer from DCS bias problems; they are not very consistent within a group; (3) If only the E-W currents from passes that contain land (so as to remove the DCS bias problem), are used, there is a smooth decrease that follows the same trend as the ground truth; (4) both the E-W INSAR estimates and the N-S INSAR estimates appear to have a 14 cm/s bias compared to the ground truth; and (5) the error in the INSAR estimates appears to be approximately 5-7 cm/s reasonably consistently (this is the standard deviation of the estimates over a large spatial region). This constant 14 cm/s bias is puzzling, since it comes from passes for which the land in the scene was used to remove any overall biases (most probably due to drift) from the scene. What is also puzzling is that the bias is the same for the N-S estimates (for which the Bragg phase speed and wind drift was removed) as the E-W estimates (for which there were no corrections at all). This indicates it is not geophysically based; however, a sensor-based reason is not obvious because the land was used to remove such biases.

To summarize the revised results: If the passes that contain land are used as an estimate of what the INSAR should do if for all the sensor-induced bias could be corrected, then the error between the INSAR data and the ground truth has a consistent mean of 14 cm/s and a standard deviation of around 5 cm/s. The 5 cm/s standard deviation is probably real and is a good estimate of how well INSAR might work in general.

4 Alternative Methods Using Synthetic Aperture Radar to Estimate Sea Surface Currents

As the above conclusion is that single antenna synthetic aperture radar interferometry will not provide useful surface current measurements (section 3.1), it is useful to consider alternative techniques for providing current information and discuss their promise. A synthetic aperture radar-based technique is discussed and followed up with a related, but non-imaging technique.

4.1 Combined AVHRR and Synthetic Aperture Radar

The possibility of combining AVHRR and synthetic aperture radar data to obtain surface currents, eddies and other ocean surface features was considered; however, attempts to correlate AVHRR thermal features with synthetic aperture radar signatures were unsuccessful due to clouds obscuring the ocean surface in the AVHRR images. Adverse weather conditions likewise precluded efforts to fuse synthetic aperture radar data with AVHRR imagery for improved estimates of surface currents.

4.2 Synthetic Aperture Radar Doppler Displacement

One technique that has been used with moderate success on Seasat synthetic aperture radar data examined the Doppler frequency shift associated with surface motions (Shuchman et al., 1981). Given the coherent nature of the recorded synthetic aperture radar data, the frequency of the returned signal is captured. This frequency will be shifted due to surface motion and thus provides a means of current measurement. The study performed by Shuchman et al. utilized an optical processing technique that isolated specific areas and examined their frequency characteristics to identify a shift associated with surface currents. This study contrasted frequency data of an ocean surface with a nearby land scene which of course is stationary. Aircraft data also

utilized in this study showed more promise than the satellite data, particularly at higher frequencies which, as discussed in the next section, are inherently more sensitive to surface motions.

The approach used by Shuchman et al. is easily implemented digitally. One can use the raw synthetic aperture radar phase history data or complex processed imagery. The technique is to perform a Fourier Transform and average the resulting spectrum over the range dimension to produce an azimuth frequency spectrum. For a stationary surface, this spectrum should be centered at zero frequency with a frequency distribution that closely mimics the antenna pattern. With a moving surface, this spectrum will be shifted in frequency due to the mean motion of the surface (Doppler shift) and broadened due to smaller-scale motion of the surface.

It was attempted to apply this same technique to a subset of the Delaware Bay Radarsat data set. Shown in Figure 15 is a Radarsat image collected on 16 January 1998 with an incidence angle of 23 degrees. Three areas where frequency measurements were performed are indicated on the image. These included a stationary land scene and two water areas on either side of what appears to be a front. Each of these areas is 1024 pixels in azimuth by 256 pixels in range representing an area of about 5 by 2 km. Each area was two-dimensionally Fourier transformed, detected, and averaged over range to produce an average azimuth frequency spectrum. For a stationary, uniform clutter scene, this would appear as the azimuth antenna pattern. For a surface moving towards the radar, the spectrum will be shifted to a higher frequency by an amount given by $(2v_r/\lambda)$ where v_r is the scatterer velocity projected along the radar line-of-sight and λ is the radar wavelength. Similarly, if the motion is away from the radar, the frequency will be shifted by a lower frequency given by the same relationship. The results for the three areas from Figure 15 are shown in Figure 16.

The magnitude of the land scene is higher because the mean backscatter is higher and image intensity was not normalized. Also, there is no apparent shift in frequency between any of these pairs which indicates little if any radial currents. As will be discussed below, the Radarsat is relatively insensitive to motion but a simple system could be constructed which would greatly increase the sensitivity to these motions.

4.3 General Radar Technique

An essential relationship for radar sensing of surface currents is given by the ratio of the frequency shift due to surface current (Doppler frequency) to the frequency spectrum width associated with the antenna and moving platform. This relationship can be reduced to

$$\frac{v_r}{\beta V} \tag{7}$$

where v_r is the radial velocity of the scatterer, β is the antenna beamwidth (λ/D, λ is the radar wavelength and D is antenna size in azimuth), and V is the platform velocity. There are four methods to improve the sensitivity to frequency shifts associated with surface currents. First, increase incidence angle so surface motion and radar line-of-sight are more closely aligned. Second, decrease the antenna beamwidth by increasing the antenna size thereby increasing the radar frequency (decreasing wavelength). Third, do both, and fourth, slow the platform velocity. For satellite applications, a steep viewing angle and high platform velocity both act to limit the synthetic aperture radar's sensitivity to surface currents.

A non-imaging technique that would have utility to Coast Guard applications would utilize a high frequency radar with a long antenna and be mounted on a slow flying aircraft. If possible, the antenna could look at different angles and, in fact, could spotlight on a particular region for 90 degrees from which an absolute (not line-of-sight) current measurement could be performed. A key to this technique is having accurate knowledge of the platform's motion and the antenna-pointing angle. In fact, prior to global navigation capabilities, aircraft would utilize a dual beam radar which used this very principle to determine their speed and drift. With the advent of high precision GPS, it is now feasible to turn this around and utilize very precise knowledge of the aircraft's velocity to determine very subtle surface currents from the radar return frequency shifts.

5 Multi-sensor Approach: Results of Literature Search

After an extensive literature search into the area of using multiple satellite approaches to measure surface currents, it was determined that there is very little information in the literature that addresses this topic directly. No references to approaches that directly merge data from multiple sensors were found; however, several ideas were considered.

The first and perhaps most obvious is multi-sensor feature tracking. This would make use of the fact that the same area can be imaged more often when using multiple systems (simply because you are no longer constrained to the orbit of a single system). With less time between successive images, there is a better chance of seeing the same feature in multiple frames. The disadvantage is that there is no guarantee that each of the available systems will image features in the same way. For example, an AVHRR scene may be cloud covered, blocking the surface, while Radarsat sees through the same clouds. Additionally, varying resolutions of the systems may complicate matters. AVHRR has a resolution of 1 km, where Radarsat has a resolution of about 25m. This limits the types of features that could be resolved in each image. In addition, suppose that some feature is identifiable and it appears to have moved over time. It is not necessarily the case that 1) the feature has in fact moved, since AVHRR and synthetic aperture radar measure such dramatically different geophysical properties; or 2) that the feature motion is correlated with surface currents (for example, the feature may be related to a thermal front). Given this, it seems unlikely that the USCG could use the multi-sensor feature tracking approach operationally.

The second and possibly more promising idea is to generate large-scale current estimates from two images and combine the results to create a more accurate current map. For example, methods of using AVHRR-based techniques to generate current estimates have been published (Emery et al., 1992; Kelly, 1992). The possibility was also discussed of using large-scale changes in radar cross section across a synthetic aperture radar image to estimate surface current from a synthetic aperture radar image based on conservation of wave action. It may be possible to combine the two approaches to generate a more accurate current estimate. One idea is to use the output of one model to set initial conditions for the second and iterate between the two models until a consistent current is found. Another approach is to simply average the results of the two techniques and use that as the current estimate. Either way, this is an area in the early stages of research and is a long way from being operationally applicable to USCG search and rescue.

6 Conclusions

Several approaches for extracting surface current information from synthetic aperture radar ocean imagery have been examined and demonstrated with differing levels of success. These methods are based on a variety of techniques, including small-scale wave-current interaction theory, long wave refraction, and feature tracking. In all cases, a lack of surface truth data hindered efforts to validate the models.

The ability to acquire, process, and interpret the data in near real-time is critical to the success of a rescue mission. Spaceborne systems are not well suited to this for several reasons. First, spaceborne systems are constrained to a particular orbit. Therefore, there is a delay, which is a function of the revisit cycle and the sensor swath, for the sensor to image the area of interest. Second, the time between acquisition of two sequential images of the same region is likely to be operationally unacceptable. Third, the amount of time between placing an image request and image acquisition is ill suited to the mission. At present, Radarsat International's "urgent" level service must be ordered two full days prior to acquisition (see Radarsat International (1995) for more information about scheduling Radarsat acquisitions). The design goal of the Radarsat Emergency Response Subscription Service (RERSS) to respond within 24-48 hours of initiating a request (Radarsat International, 1998) is unsatisfactory for most search scenarios. Fourth, without a real-time link, image delivery can take hours to days.

The question of whether a single antenna INSAR technique could provide current information was investigated and was shown infeasible. A discussion on what radar parameters determine its sensitivity to surface currents was presented along with concepts on how a single antenna non-synthetic aperture radar system could be used to support Coast Guard operations.

The results of an airborne INSAR data collection and analysis were also presented. The initial comparison with ground truth was very poor. Further processing and re-analysis of the data produced a significantly better agreement but led to grave concerns over the reliability and operational accuracy of the INSAR data.

Alternative satellite methods for current determination were briefly evaluated and quickly concluded that the techniques considered held little promise.

At present, satellite synthetic aperture radar is not feasible for operational Coast Guard search planning. Immediate on-scene data cannot be obtained due to Radarsat's orbit, ordering requirements and data delivery delays. Sea surface current information can not be reliably extracted from single antenna systems. Ocean monitoring is not an option because of the Coast Guard's enormous operating area and cost considerations.

7 Recommendations

Due to the time and areal constraints of a CG search and rescue case, space-borne oceanographic synthetic aperture radar remote sensing should not be considered a viable option at this time. Improvements in resolution, data transmission and processing rates, data analysis techniques and the availability of satellite sensors are necessary and are likely in the near future.

Initial optimism for airborne remote sensing was not confirmed by field exercises. Airborne sensing is limited in its areal coverage, by weather constraints, and by processing difficulties.

Therefore, it is recommended at this time that the CG does not implement either satellite or airborne synthetic aperture radar remote sensing for search and rescue missions. It is, however, recommended that the CG maintain a noticeable and vocal presence in the remote sensing community, governmental and industry, nationally and internationally, to encourage and motivate the research in operational oceanographic remote sensing. Remote sensing appears to be a tool without an obvious and feasible oceanographic purpose. The CG has a significant need for near real-time oceanographic data that can only be provided by remote sensing. By steering research into the direction of our needs, the solution will be obtainable.

8 References

Banner, M.L. and O.M. Phillips, On the incipient breaking of small scale waves. J. Fluid Mechanics, 65 (4), 647-656.

Bogden, P. (1999) Report to A&T: Surface Current Estimates from Shipboard ADCP Data, Unpub. USCG R&D Center Rep., 15pp.

Bogden, P. and J. O'Donnell (1998), J. Marine Research, Vol. 56, pp. 995-1027.

Dick O'Donnell, J.E. (1996) Satellite Remote Sensing for USCG Search and Rescue Planning: Present Status and Future Direction, letter report, R&DC.

Dick O'Donnell, J.E. (1998) Operational Ocean Search and Rescue Using AVHRR: Cloud Limitations, Journal of Atmospheric and Oceanic Technology, Vol. 16, No. 3, pp. 388-393.

Dick O'Donnell, J.E. and R.Q. Robe (1996) Potential of Advanced Very High Resolution Radiometer Derived Sea Surface Currents for U.S. Coast Guard Search and Rescue Application, Final Rep., U.S. Coast Guard Res. and Dev. Center, 95 pp.

Dick O'Donnell, J.E. and R.Q. Robe (1997) Application of AVHRR Imagery for Oceanic Search and Rescue, J. of Marine Tech. Soc. In review.

Dick, J.E. (1992) ISARC Project Acquires Satellite Receiving Station, On Scene 3/92, USCG, US Dept. of Trans. COMDTPUT P16100.4, 28-29.

Dick, J.E. (1994) Status Report: Search and Rescue Applications of Real-Time Satellite Imagery, letter report submitted to Commandant (G-NRS-1) via Commandant (G-ER) by CO, R&DC.

Emery, W.J., C. Fowler, C.A. Clayson (1992) Satellite-image-derived Gulf Stream currents compared with numerical model results, Journal of Atmospheric and Oceanic Technology, 9, 286-304.

Goldstein, R.M. and H.A. Zebker (1987) Interferometric radar measurement of ocean surface currents, Nature, 328, 707-709.

Goldstein, R.M., T.P. Barnett, and H.A. Zebker (1989) Remote sensing of ocean currents. Science, 246, 1282-1285.

Graber, H.C. B.K. Haus, L.K. Shay, and R.D. Chapman (1996) HF radar comparisons with moored estimates of current speed and direction: Expected differences and implications. J. Geophys. Res., (submitted).

Graber, H.C., D.R. Thompson, and R.E. Carande (1996) Ocean surface features and currents measured with synthetic aperture radar interferometry and HF radar. J. Geophys. Res., 101:C11, 25813-25832.

Jensen, J.R. and R.D. Chapman (1990) Single Antenna Interferometry, The Johns Hopkins University Applied Physics Laboratory, Memo S1R-90U-044.

Johannessen, J.A., R.A. Shuchman, G. Digranes, D.R. Lyzenga, C. Wackerman, O.M. Johannessen and P.W. Vachon (1996) "Coastal ocean fronts and eddies imaged with ERS 1 synthetic aperture radar," Journal of Geophysical Research, Vol. 101, pp. 6651-6667.

Kelly, K.A. (1992) Comparison of velocity estimates from advanced very high resolution radiometer in the coastal transition zone, J. Geophys. Res., 97, 9653-9668.

Kramer, H. J. (1996) Observation of the Earth and its Environment: Survey of Missions and Sensors 3rd Ed., Belin, Springer.

Lyzenga, D. R. (1991) Interaction of short surface and electromagnetic waves with ocean fronts, J. Geophys. Res., 96, 10,765-10,772.

Lyzenga, D. R., and N. P. Malinas (1994) Airborne radar measurements of coastal ocean currents and waves, Second Thematic Conf. on Rem. Sens. for Marine and Coastal Env., New Orleans, LA.

Lyzenga, D.R. and N.P. Malinas (1994) Azimuth falloff effects in two-antenna SAR measurements of ocean wave spectra, IEEE Trans. Geosci. and Rem. Sens., 34, 1020-1028.

Miller, D., C. Wackerman and E. Ericson (1997) Estimation of Ocean Surface Currents Using Radarsat Synthetic Aperture Radar, Environmental Research Institute of Michigan, Ann Arbor, MI, Prepared for: Maritime Operations Technology Division, U.S. Coast Guard Research & Development Center, Groton, CT.

Miller, D., C. Wackerman, R. Perigo, D. Lyzenga and J. Lyden (1999) Assessment of Synthetic Aperture Radar (SAR) for United States Coast Guard Search Planning, Environmental Research Institute of Michigan, Ann Arbor, MI, Prepared for: Maritime Operations Technology Division, U.S. Coast Guard Research & Development Center, Groton, CT.

O'Donnell, J. (1999) An Evaluation of the Interferometric SAR Estimates of Ocean Surface Currents: Final Report, Unpub. USCG R&D Center Rep., 21pp.

Plant, W.J. (1986) "A twoscale model of short wind waves and scatterometry," Journal of Geophysical Research, Vol. 91, pp. 10735-10749.

Radarsat International (1995) RADARSAT Illuminated: Your Guide to Products and Services, Published by Radarsat International Client Services.

Radarsat International (1998) "RADARSAT Emergency Response Subscription Service," Reflections, Vol.7, No. 1, p. 6.

Raney, R. K. (1971) Synthetic aperture imaging radar and moving targets, IEEE Trans. Aero. and Electr. Systems, 7, 499-505.

Shemer, L., M. Marom and D. Markman (1993) Estimates of currents in the nearshore ocean region using interferometric synthetic aperture radar, J. Geophys. Res., 98, C4: 7001-7010.

Shuchman, R.A., D.R. Lyzenga, and A. Klooster (1981) Exploitation of SAR Data for Measurement of Ocean Currents and Wave Velocities, ERIM Final Report No. 137600-1-F.

Thompson, D.R. and J.R. Jensen (1993) Synthetic aperture radar interferometry applied to ship generated internal waves in the 1989 Loch Linnhe experiment. Journal of Geophysical Research, 98, 10259-10269.

Valenzuela, G.R. (1978) "Theories for the interaction of electromagnetic and oceanic waves – A review," Boundary Layer Meteorology, Vol. 13, pp. 61-85.

Wright, J.W. (1966) "Backscattering from capillary waves with application to sea clutter," IEEE Trans. Ant. And Prop., Vol. 14, pp.749-754.

Wright, J.W. (1968) "A new model for sea clutter," IEEE Trans. Ant. And Prop., Vol. 16, pp. 217-223.

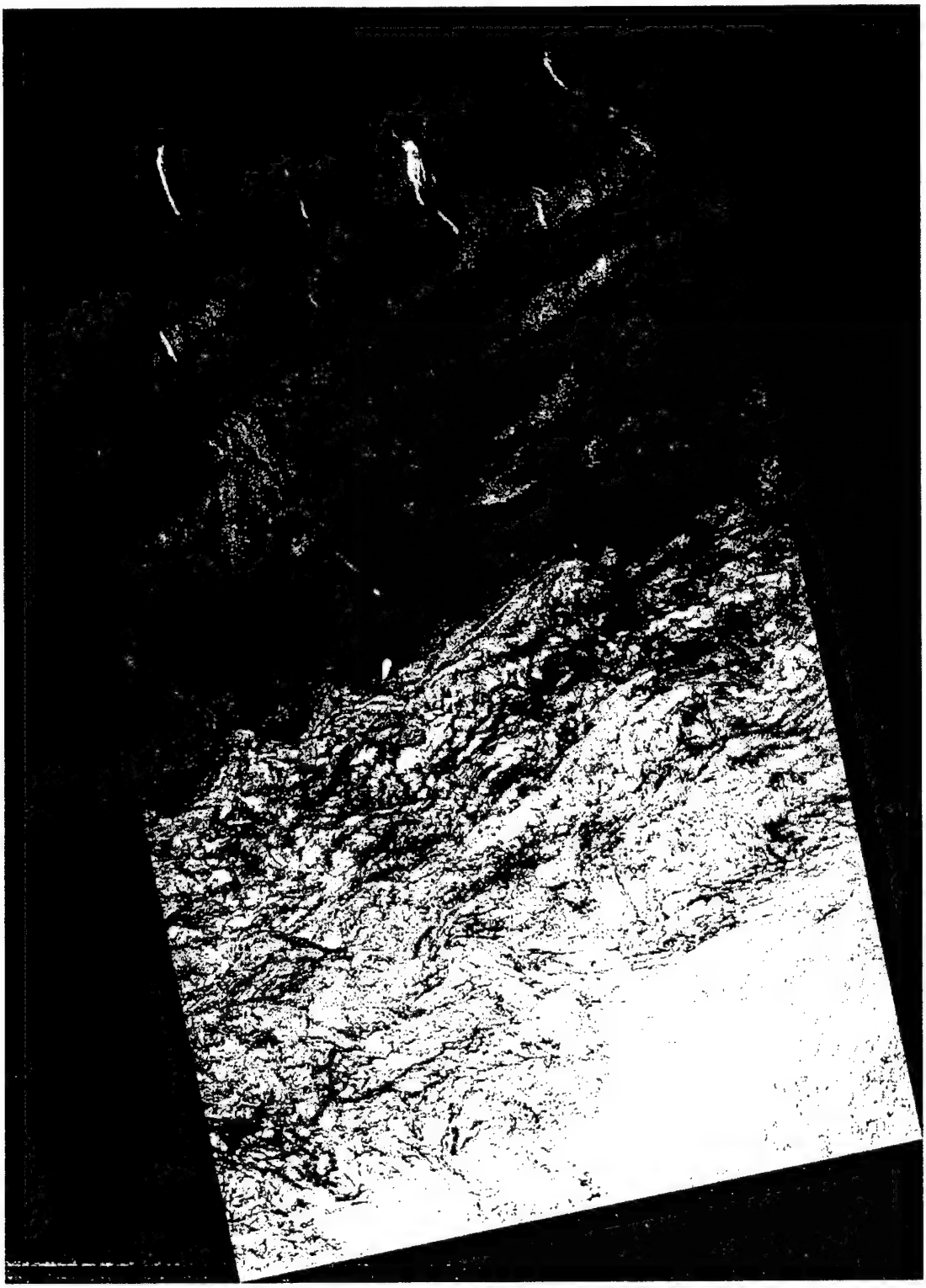

Figure 1. Radarsat image of Georges Bank, 2 June 1996, shows areas of high and low backscatter.

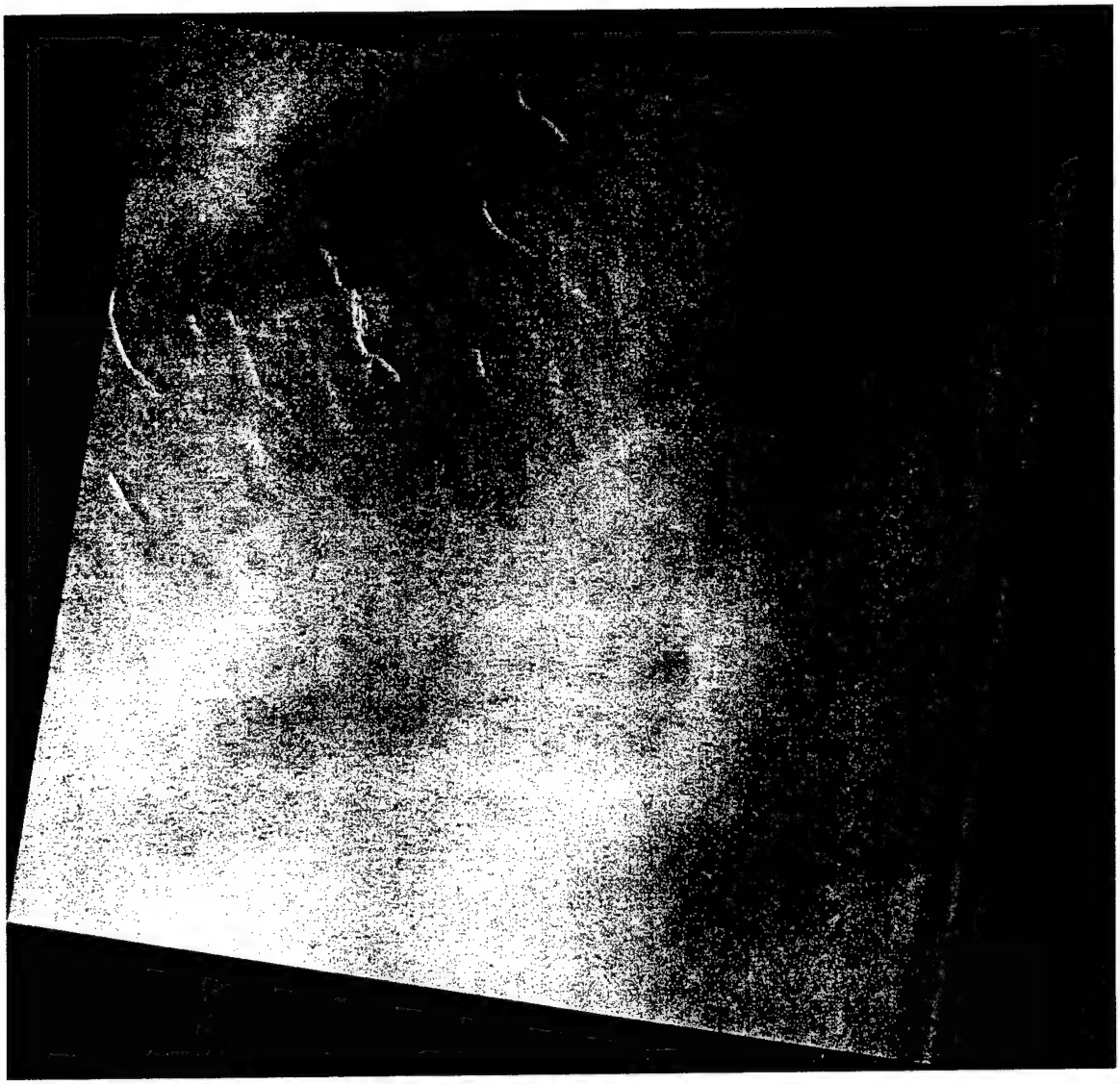

Figure 2. Synthetic aperture radar image over Georges Bank on 3 June 1996.

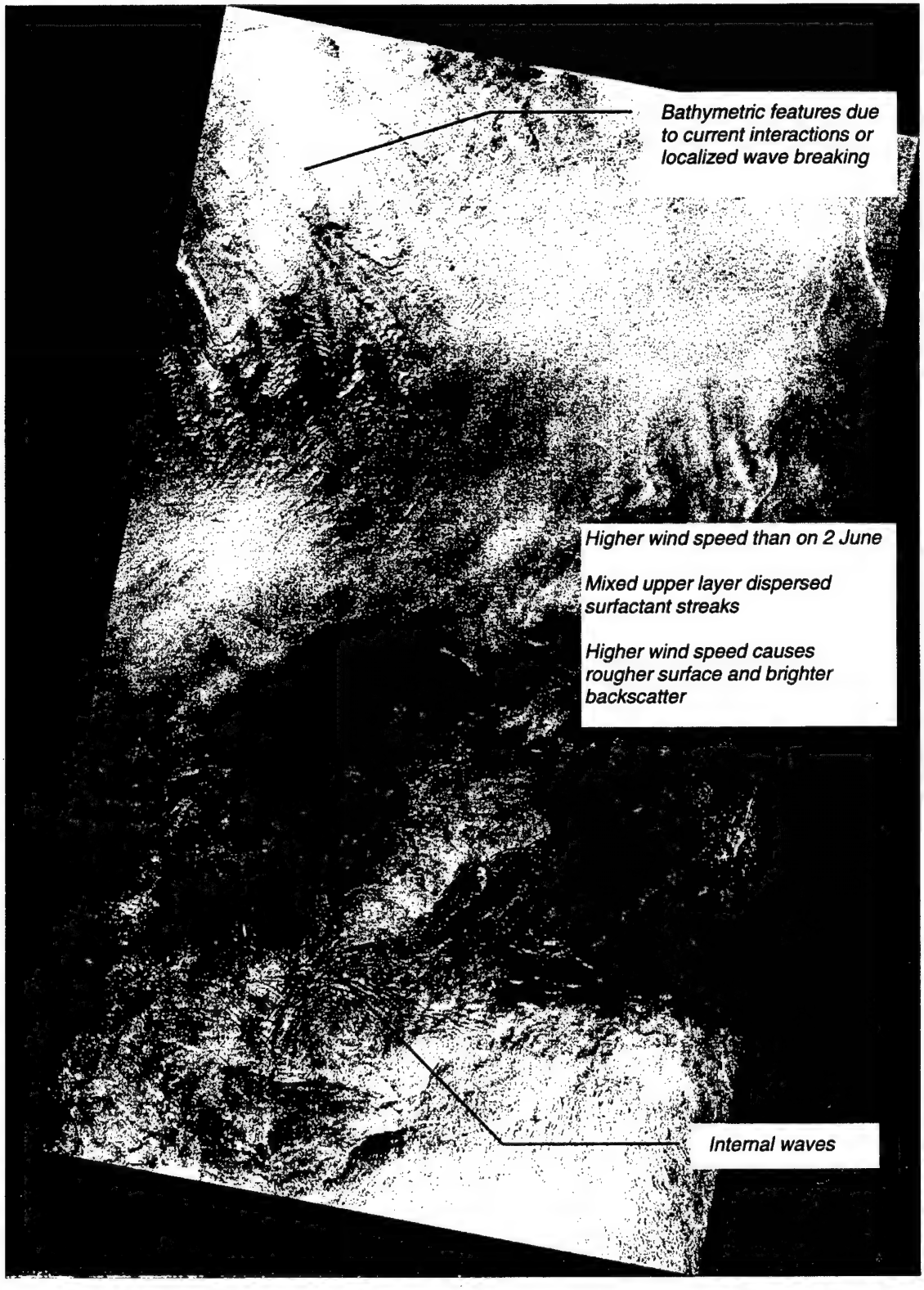

Figure 3. Radarsat synthetic aperture radar image over Georges Bank on 13 June 1996 shows synthetic aperture radar signatures of surface features.

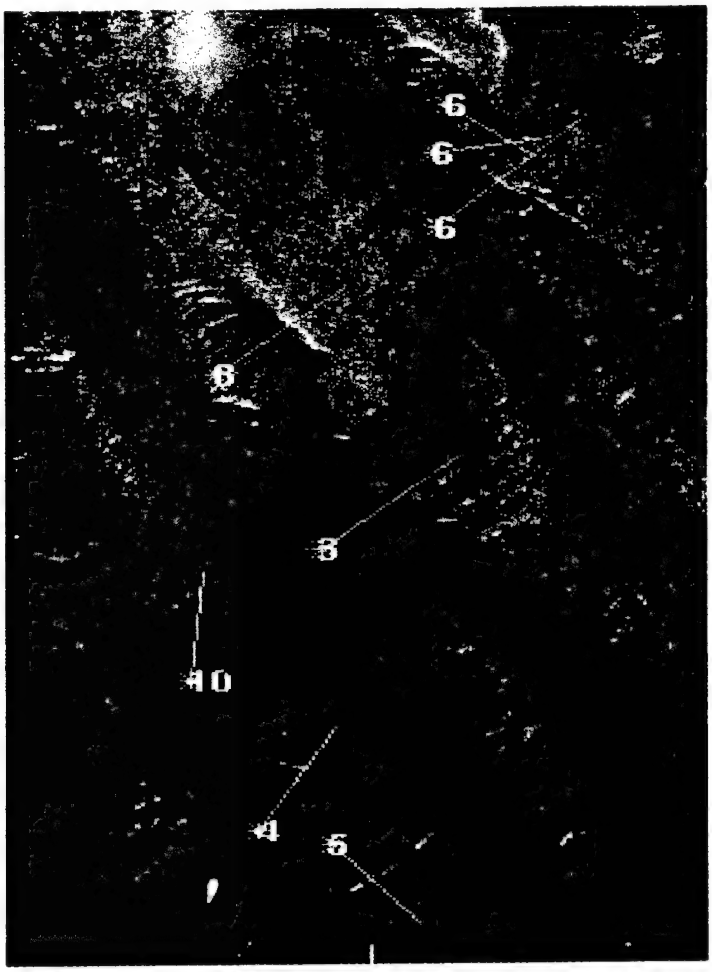

Figure 4. The results of estimating the RCS across the features in the upper left portion of the image shown in Figure 3. This image shows the primary direction of current flow over each scan region.

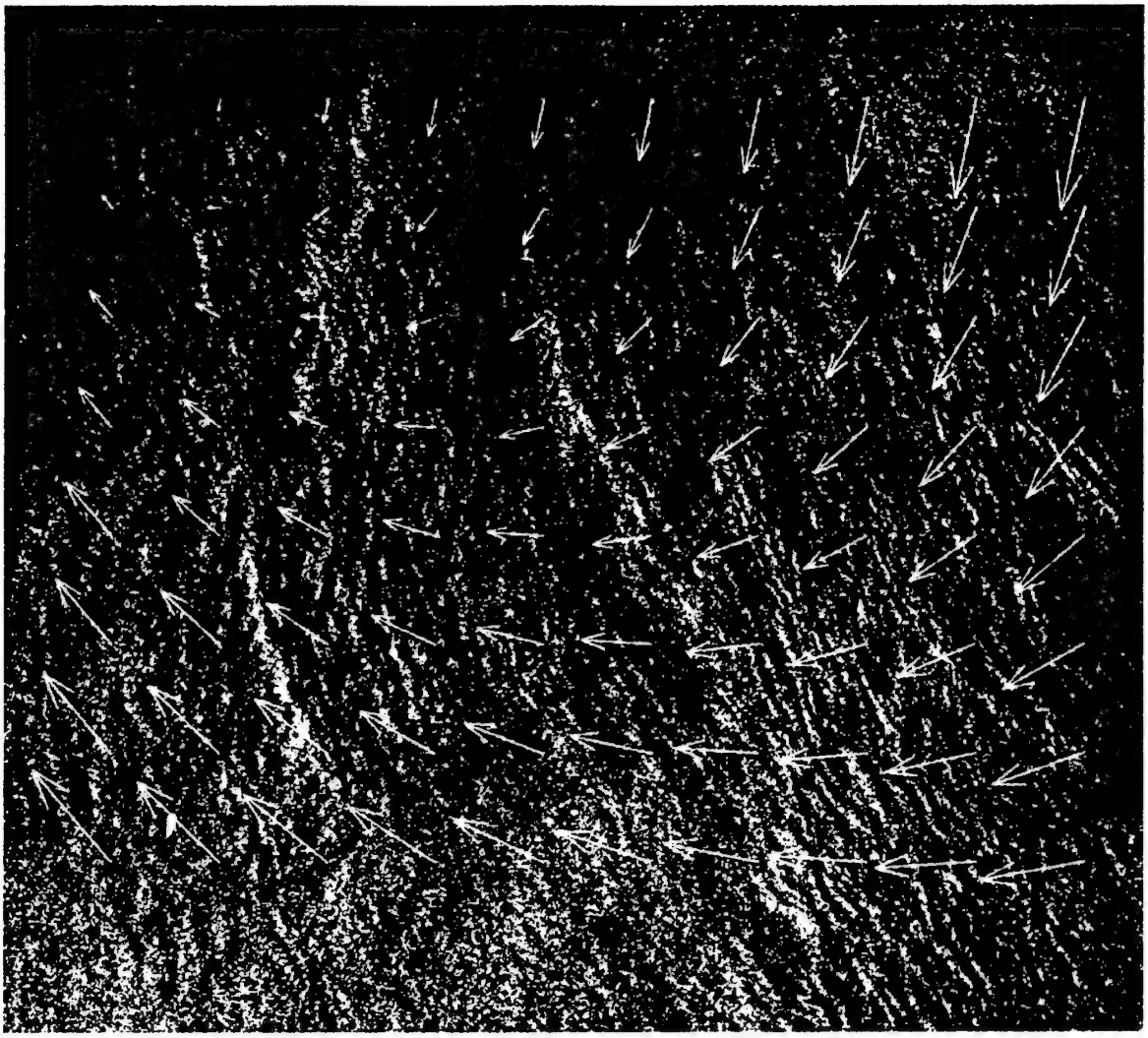

Figure 5. Computed current field for region of Figure 3. The initial current guess for this image was 0.

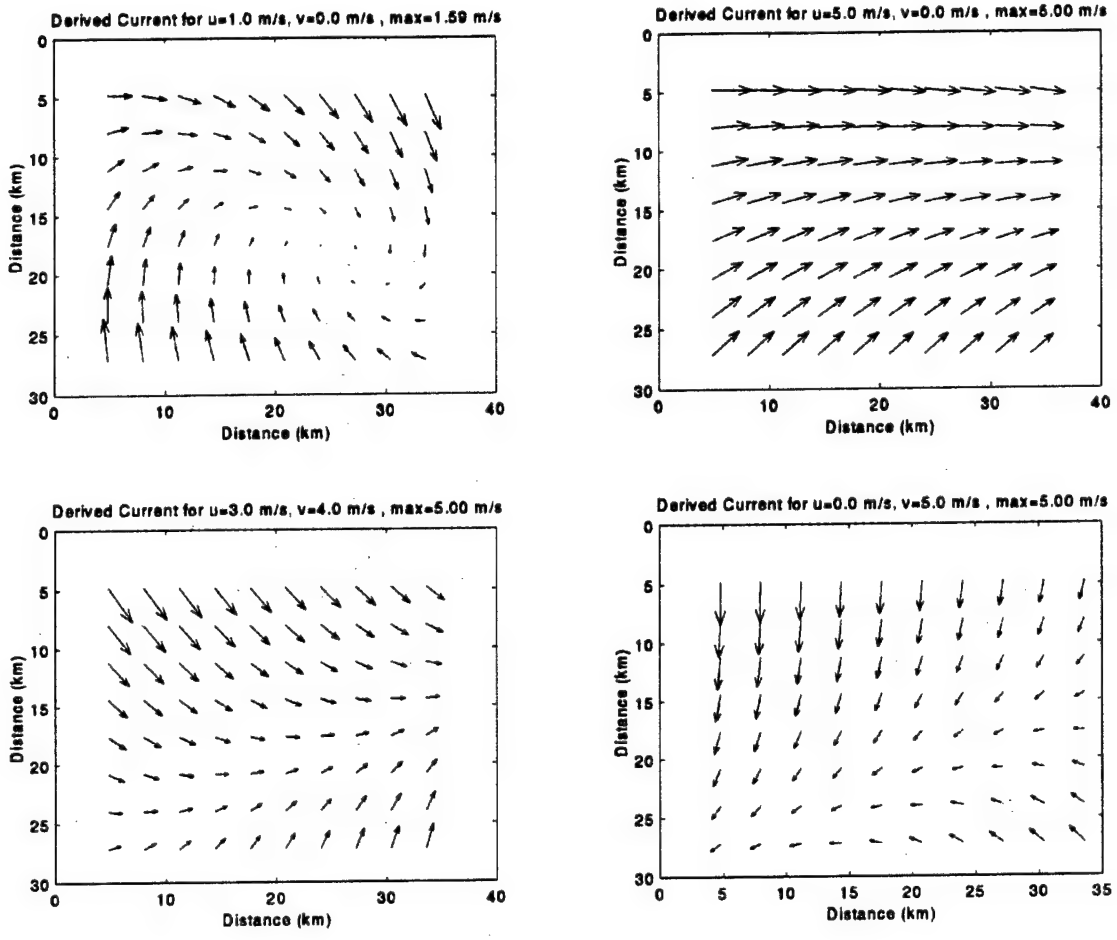

Figure 6. Four panels (a-d reading right to left first) showing different current fields based on different initial conditions. Note that each of these estimates is consistent with the wave field shown in Figure 5.

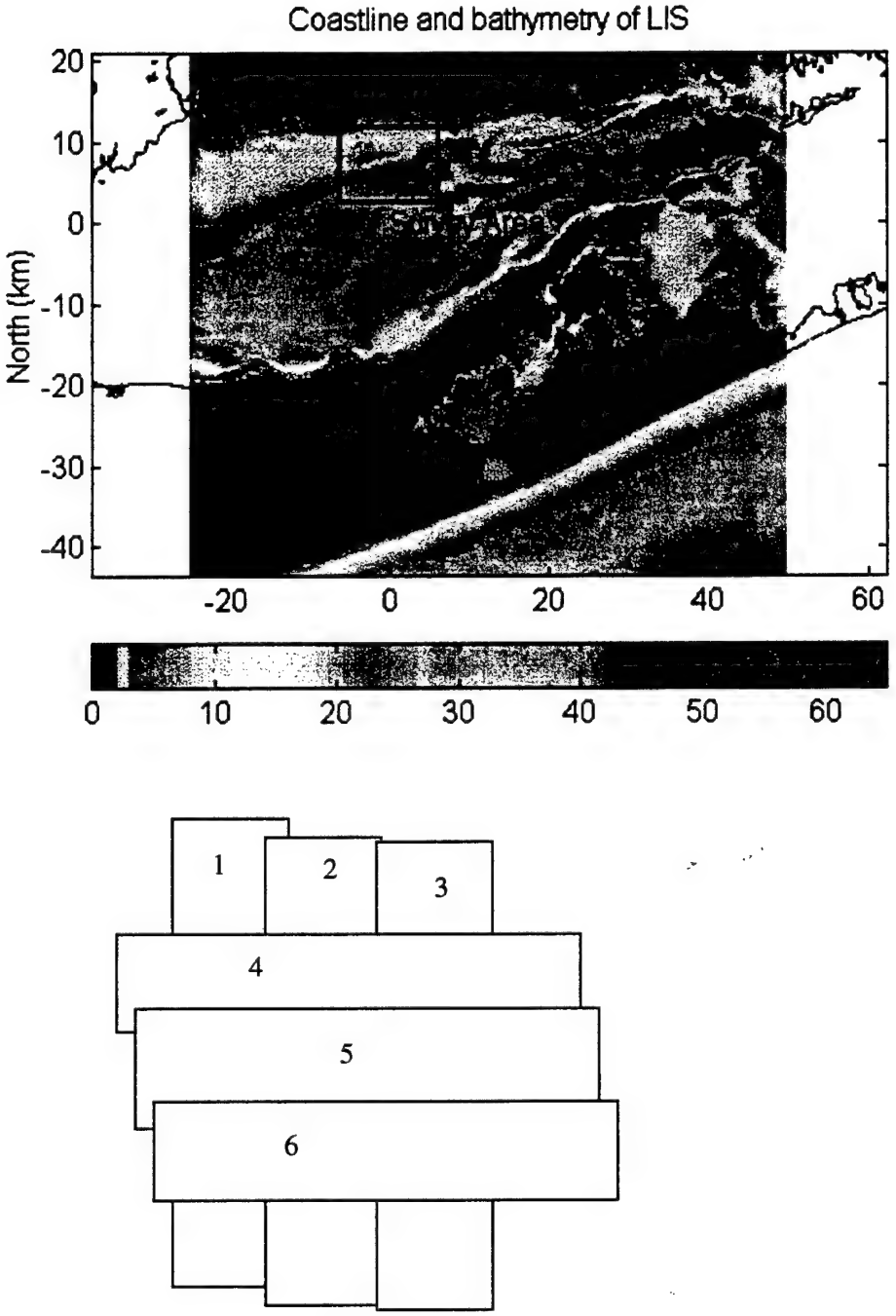

Figure 7. Map of the eastern half of Long Island Sound showing the test area in the vicinity off Falkner's Island (upper frame) and a graphical depiction (not to scale) of INSAR DCS collection pattern over Long Island Sound (lower frame).

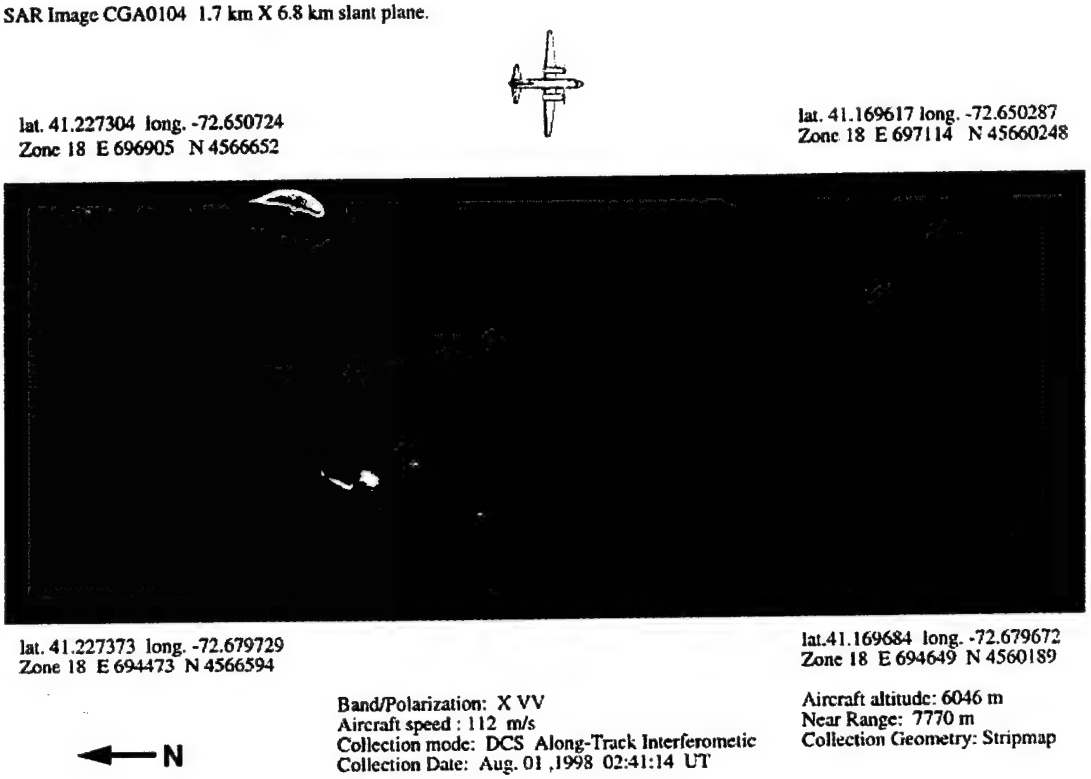

Figure 8. Example of INSAR DCS image from pass 4. This is a magnitude image only from a single antenna and does not contain any current information. The bright areas are islands.

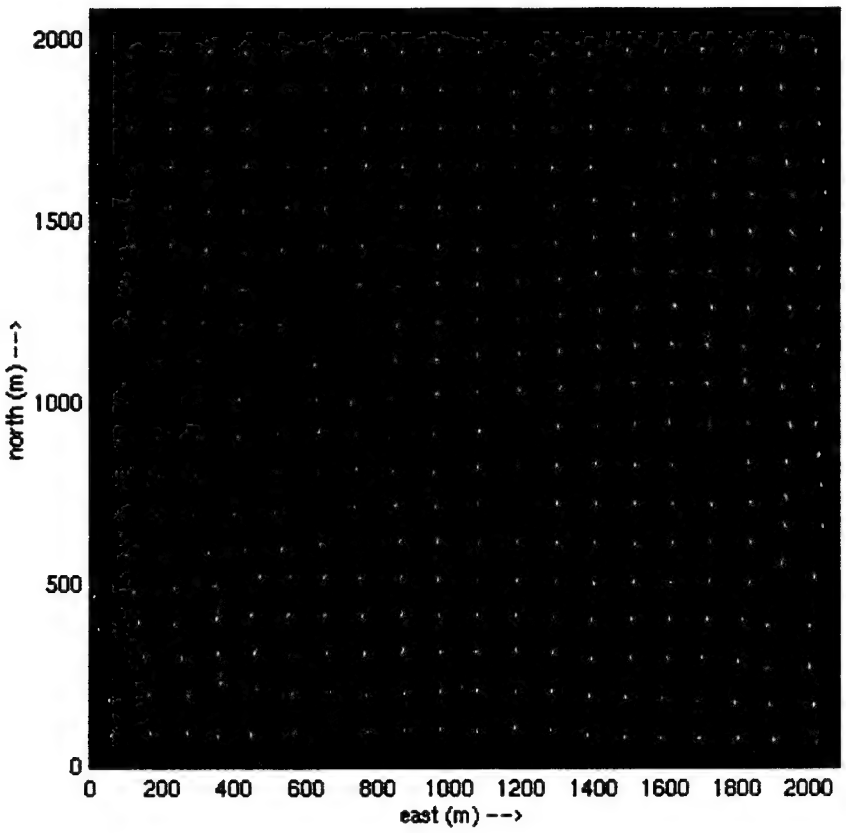

Figure 9. Current estimates depicted as vectors overlaid on the image from the E-W pass. The length of the vector is scaled to the peak current magnitude (0.92 m/s) with direction indicated by the arrow.

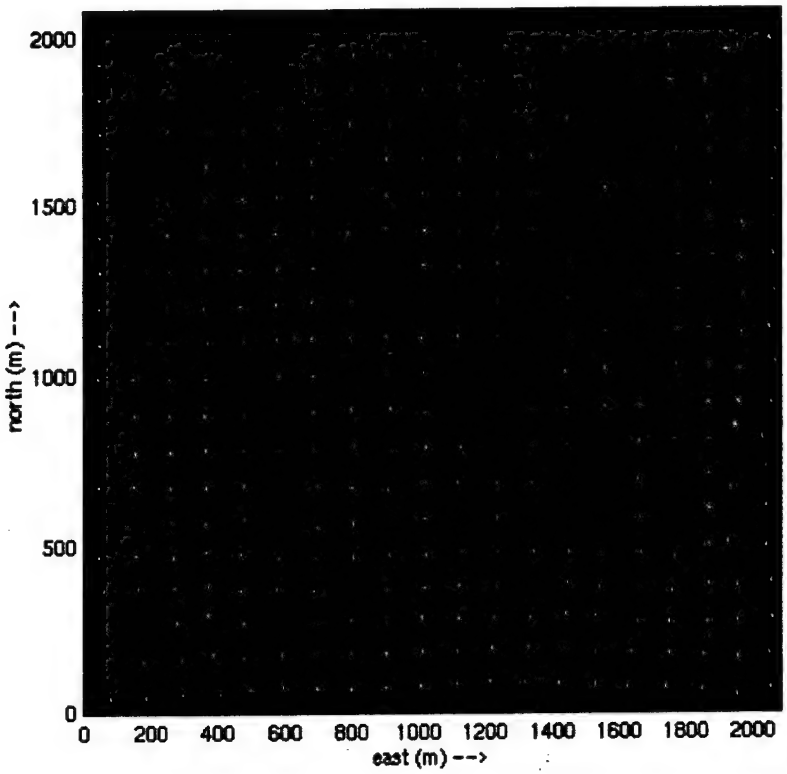

Figure 10. Currents calculated for the same spatial coverage based on images collected approximately three hours later and therefore under different tidal conditions.

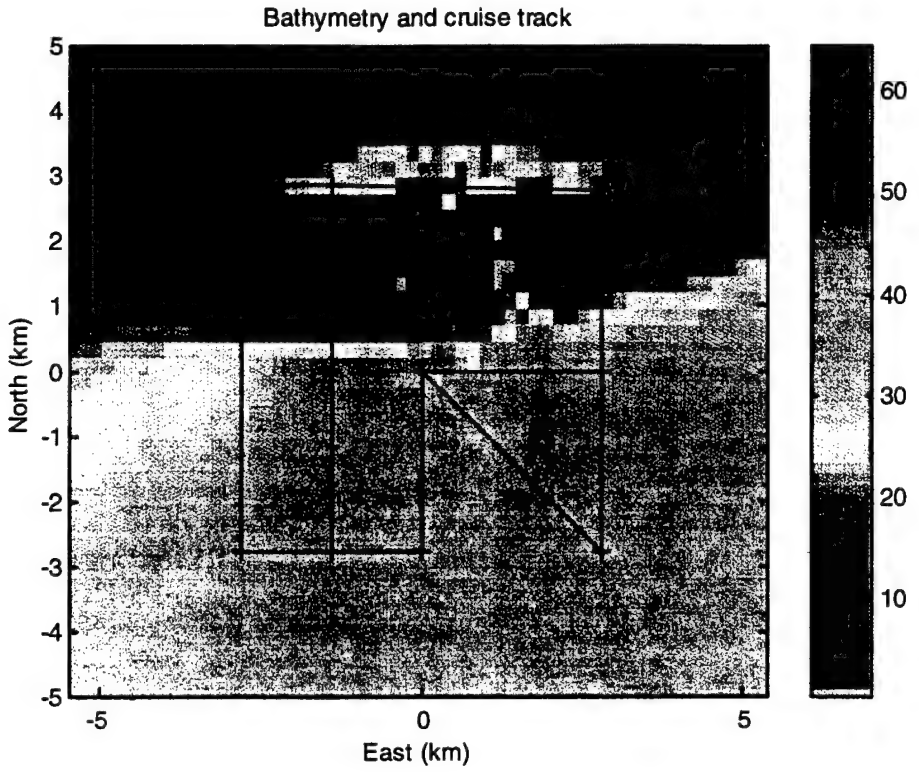

Figure 11. Map showing the bathymetry and R/V UConn cruise track. Bathymetry in meters.

(a)

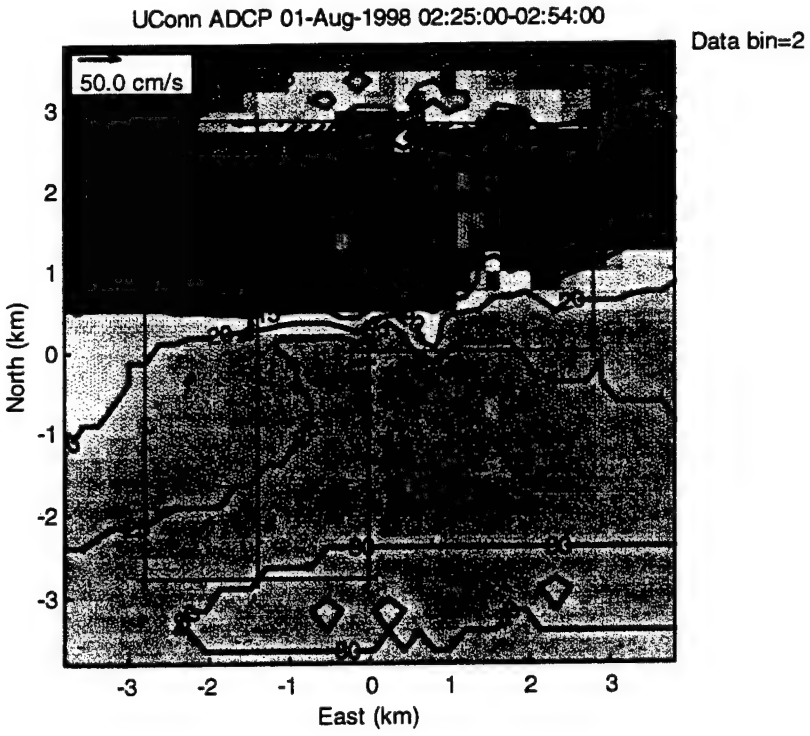

(b)

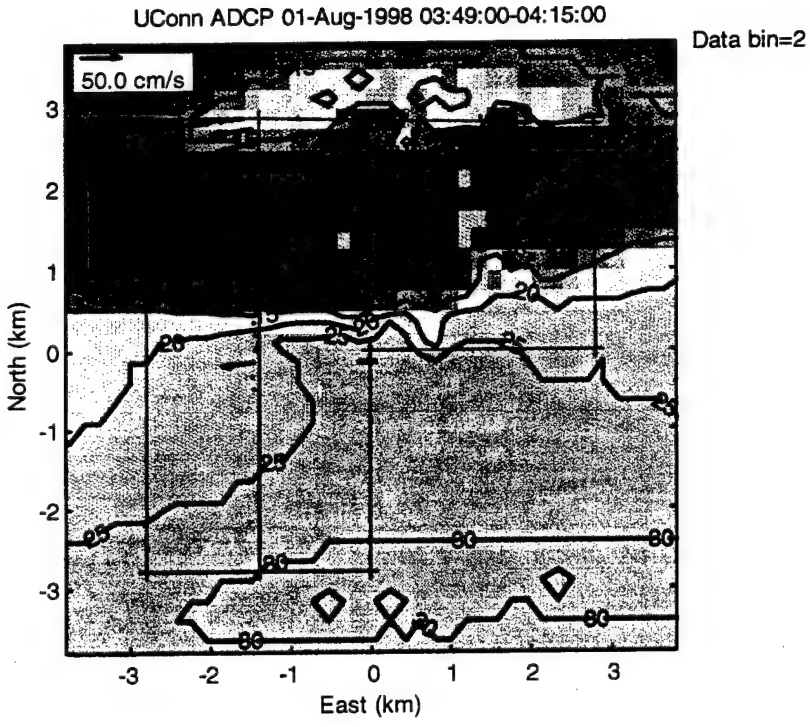

Figure 12. ADCP observations in a 0.35-m vertical bin centered at 1.3 m below the surface are shown as vectors superimposed on the bathymetry of the survey area. The depth contours are in meters below the surface. Estimates were obtained between (a) 02:25 and 02:54 and (b) 03:49 and 04:15 on August 1, 1998.

(c)

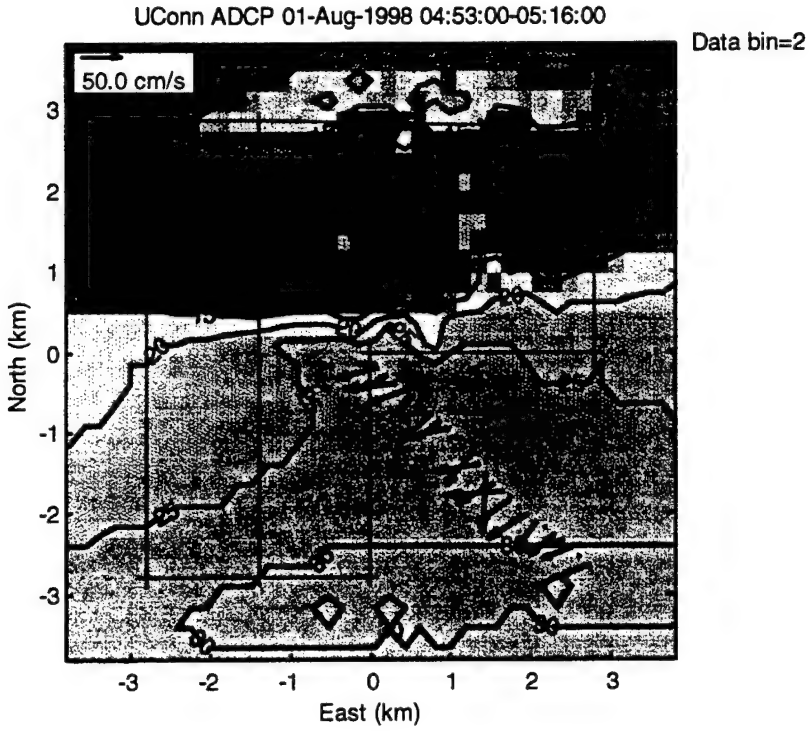

(d)

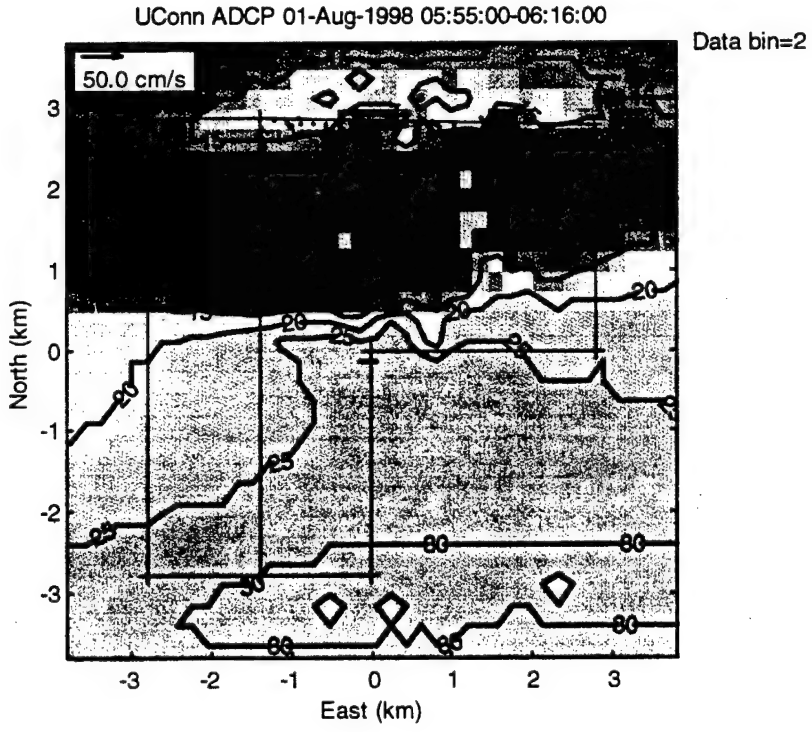

(continued). ADCP observations obtained between (c) 04:53 and 05:16 and (d) 05:55 and 06:16 on August 1, 1998.

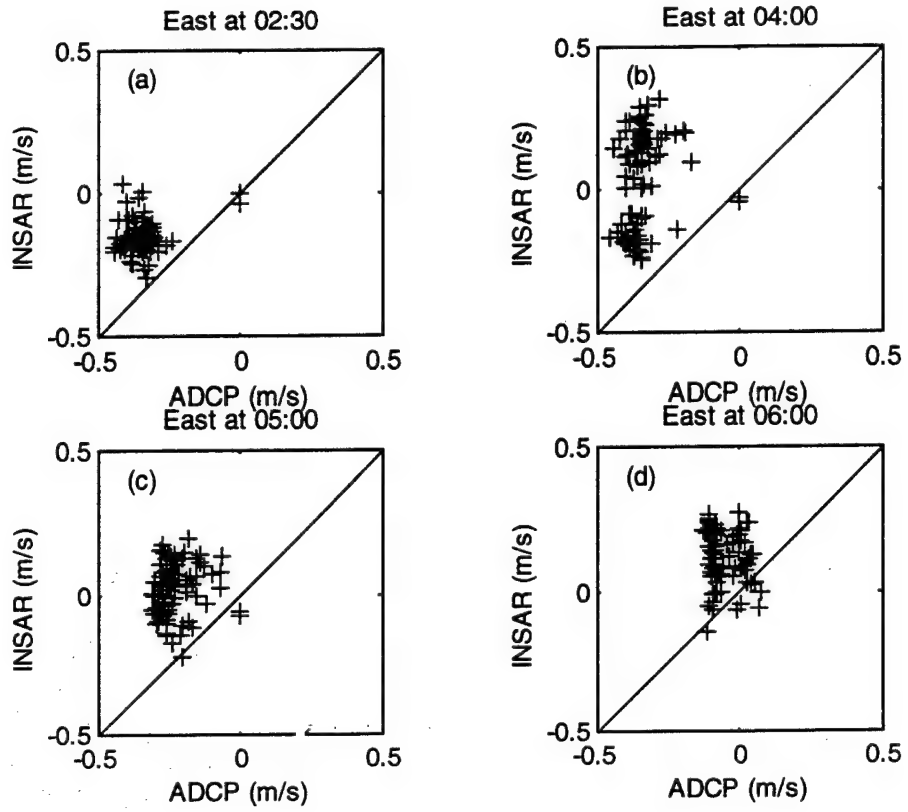

Figure 13. Correlation of the east components estimated by the analysis of the ADCP data and the INSAR system.

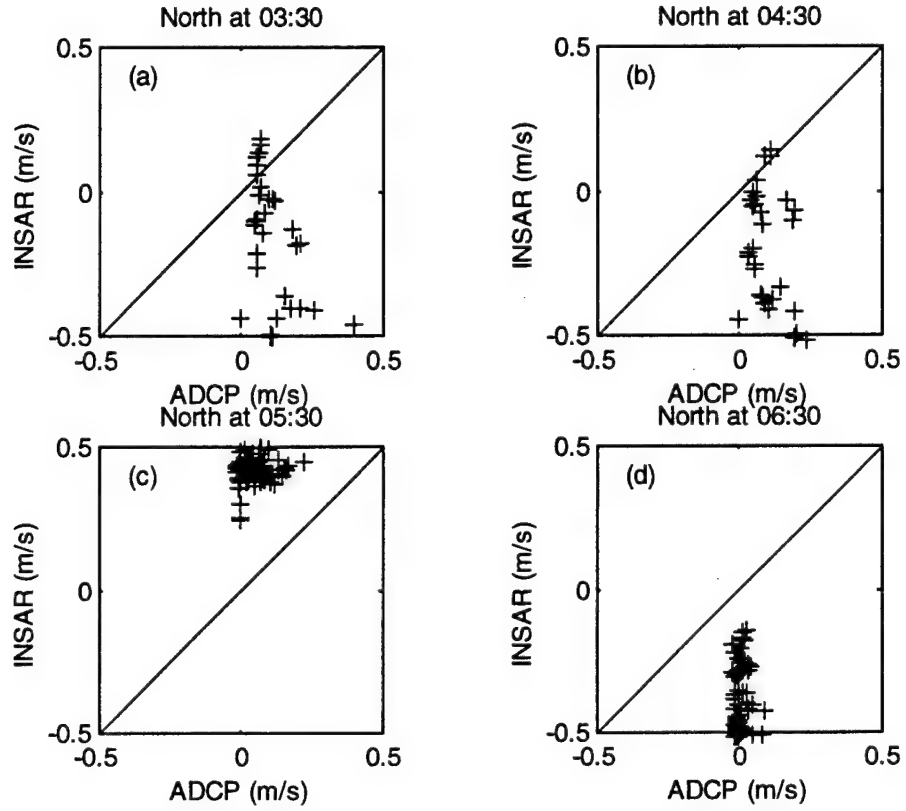

Figure 14. Correlation of the north components estimated by the analysis of the ADCP data and the INSAR system.

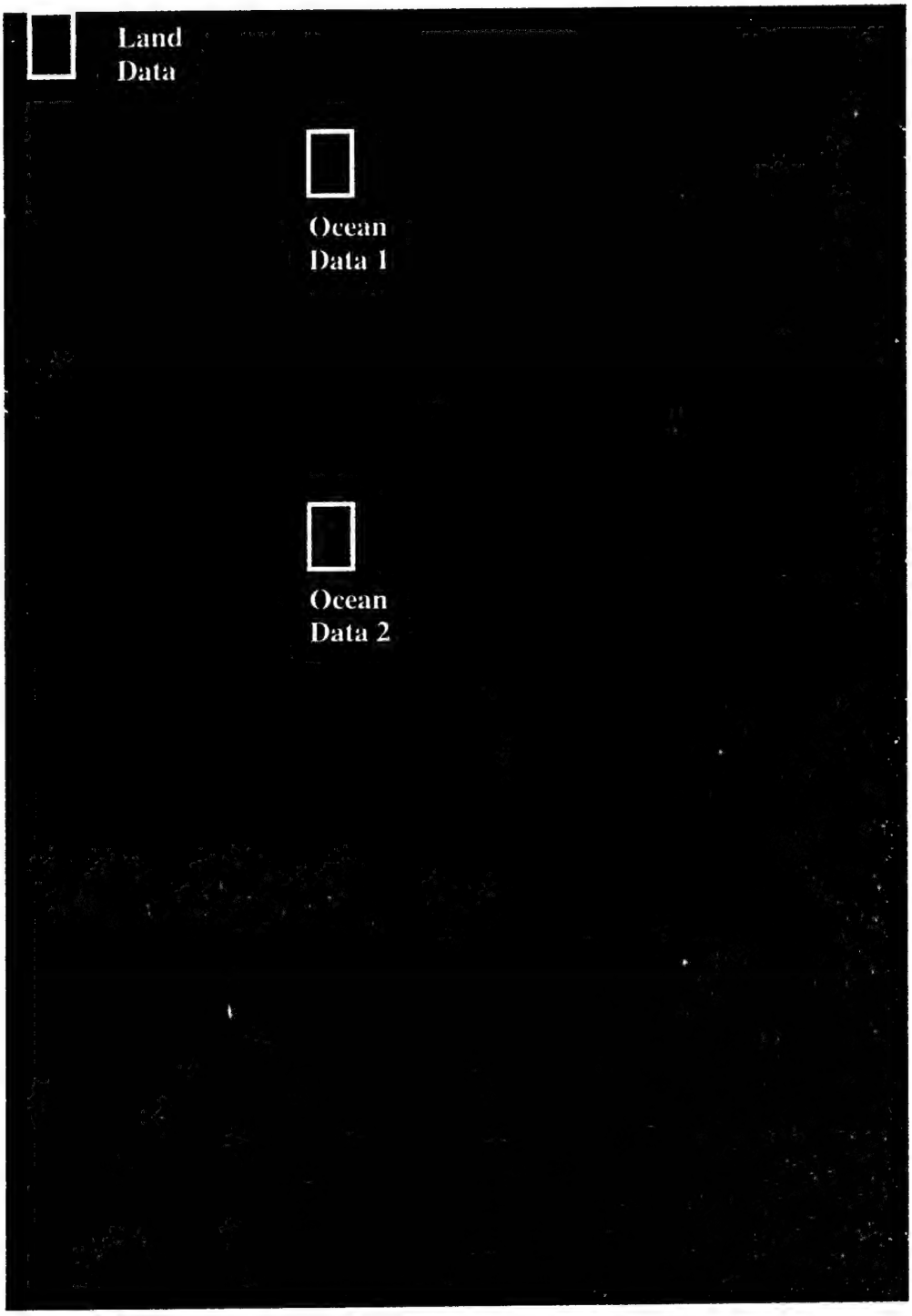

Figure 15. Radarsat image collected on 16 January 1998 off Delaware Bay indicating the three areas where Doppler spectrum measurements were performed. Azimuth is in the vertical dimension and range is horizontal.

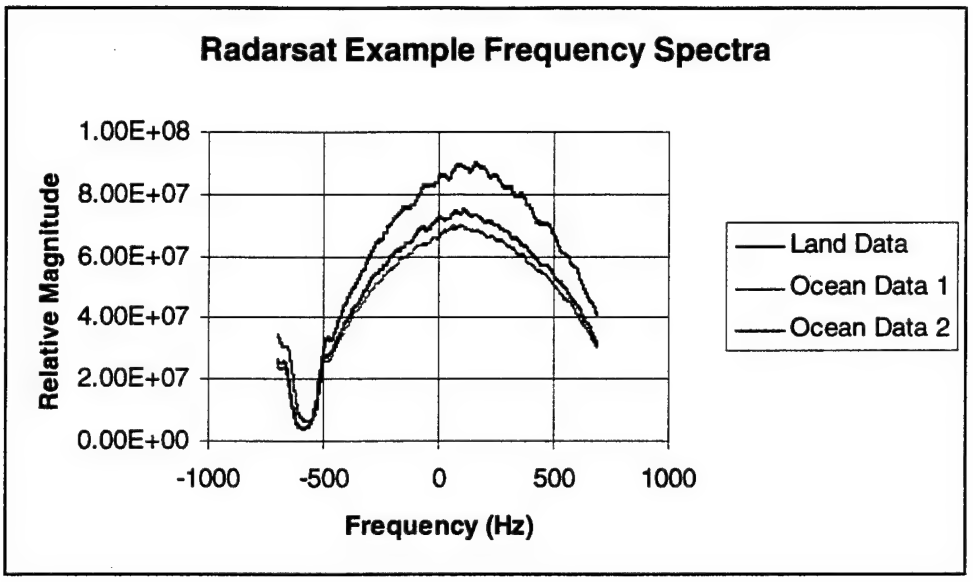

Figure 16. Example frequency spectra from Delaware Bay Radarsat image. The upper trace is for a stationary land scene while the lower traces are from two different ocean areas. The two ocean traces are not shifted significantly from the land trace indicating little if any current components in the radar line of sight. The near identical nature of the two ocean areas indicates little if any change in the current components in the radar line-of-sight between these two areas.

Table 1. Radarsat SAR passes acquired during Georges Bank field test.

Date	Time, UTC	Node Direction	Beam Mode
2 June 96	22:23:41	Ascending	Standard-3
3 June 96	10:36:28	Descending	Wide-1
13 June 96	10:44:49	Descending	Standard-1

Table 2. Summary of published INSAR validation studies including the date, system and surface truth used for comparison.

Date/Location	System	Surface Truth	Reference
16 April 1988 San Diego, CA	AIRSAR	Drifters	Goldstein, *et al.*, 1989
1989 Loch Linnhe	AIRSAR	Current Meters (projected to surface)	Thompson and Jensen, 1993
8 September, 1989 Monterey Bay, CA	AIRSAR	Drifters	Shemer *et al.*, 1993
June 20, 1993 Cape Hatteras, NC	AIRSAR / P3-SAR	HF RADAR	Graber *et al.*, 1996

Table 3. INSAR survey times on August 1, 1998.

Survey	Component	Start	End
1	East	2:25:31	2:53:59
2	North	3:17:13	3:38:29
3	East	3:49:15	4:15:25
4	North	4:22:22	4:45:48
5	East	4:53:28	5:47:30
6	North	5:25:26	5:47:30
7	East	5:55:46	6:16:29
8	North	6:27:49	6:48:59

Appendix A: Cost Pertaining to INSAR Systems

There are currently only a few suppliers of commercial interferometric Synthetic Aperture Radar (INSAR) systems that could supply a complete system to meet the needs and requirements of the U.S. Coast Guard. This include ERIM International in Ann Arbor, Michigan; MacDonald Dettwiller in Vancouver, British Columbia, Canada; and Daimler-Benz in Germany.

Figure 1 – Typical Interferometric Synthetic Aperture Radar Installation In A Learjet 36

(Photo Courtesy Of ERIM International)

Generally these systems are installed and operated on small to mid-sized commercial business jets or turbo-props. A Learjet 36 installation is shown in Figure 1. Installation in a C130 or HU-25 Falcon Jet would be a reasonable approach. The installation is typically in a belly-mounted radome and requires fairly extensive aircraft modifications for the radome, racks, and power generation/distribution. All products being offered by these suppliers are based heavily on the use of COTS equipment.

Nominal sets of performance parameters for an airborne INSAR system are listed in Table 1. These specifications are for existing EI systems. A system designed to measure surface currents

would not vary appreciably from the parameters in table 1. The most notable variations would be in polarization (a surface-current measuring system would be VV, not HH) and in the relative position of the antennas (current are measured with antennas separated in the along-track rather than across-track direction). Neither of these changes affects the cost appreciably.

Table 1 – Typical INSAR Performance Parameters for EI Systems

PERFORMANCE PARAMETER	*EI INSARE (ACTUAL)*	***EI INSARE PLUS***	***EI INSARE II***
Frequency Band	X-Band	X-band	X-Band
Polarization Vs. Mode - INSAR - Imaging (Non-INSAR)	HH Not Applicable	HH Not Applicable	HH Variable
Nominal Operating Altitude (m)	6,000 or 12,000	6,000 to 12,000	6,000 to12,000
Data Collection Mode & Look Direction	Stripmap Left or Right	Stripmap Left or Right	Stripmap Left or Right
Ground Swath (km)	5 or 10	7.5 or 15	5 to 20
Slant Plane Resolution (m)	1.25 or 2.5	1.25 or 2.5	1.0 or 2.0
DTE Post Spacing (m)	7.5 or 15	5 to 25	5 to 25
Horizontal Position Accuracy / One Sigma (m)	1.5 or 3.0	1.25 or 2.5	1.0 or 2.0
Collection Rate $(km^2/hr)^3$	3,000-6,000	3,750-7,500	2,500-10,000
Recording Device	Ampex DCRSi-107	Ampex DCRSi-240	Ampex DCRSi-240
On-Board Image Formation Processing	None	None	Realtime Survey Image Processor (Single Channel)
Ground Processor	Fixed Ground Station	Transportable For Field Processing	Transportable For Field Processing
Number Of Non-Coherent Summed Azimuth Looks	2 or 4	2 or 4	2 or 4

Processing Throughput (km^2/hr)	60-120	400-800	1,250-2,500
Airborne Radar Equipment Volume (m^3)	0.75	0.75	0.75
Airborne Radar Equipment Weight (kg)	325	350	400
Ground Processor Equipment Volume (m^3)	0.43	0.31 / 0.46[5]	0.31 / 0.61[5]
Ground Processor Equipment Weight (kg)	140	120 / 150[5]	130 / 190[5]
Aircraft Type	Learjet 36	Business Class	Business Class

Table I Notes Appear On The Top Of The Next Page

Table I Notes

1. 1 meter without ground control points at 6,000 meter altitude over 5k m swath or 1 meter without ground control points at 10,000 meter altitude over 10 km swath.
2. 1 meter without ground control points at 10,000 meter altitude over 15 km swath.
3. Assumes 500km/hr aircraft velocity.
4. Derived from the 30,000km^2/flight capacity requirement.
5. The first value indicates the "transportable" portion of the processor that does not include the additional workstations required to accommodate the full throughput rate. The second number is for the complete processor that is capable of full throughput.

Typical procurement costs for INSAR systems are listed in Table 2 and generally include costs to modify the host aircraft and install/test the radar. Various options exist for data processing including the capability to process and display a single channel or interferometric radar image onboard the aircraft in real-time.

Table 2 – Estimated Procurement Costs

Baseline Program	**Estimated Price (US$)**
Item 1 – Airborne INSAR System	$4.0M to $6.0M
Item 2 – Aircraft Modifications	$1.0M to $1.5M
Item 3 – Aircraft Installation & Integration	$1.0M to $1.5M
Total Estimated Cost	**$6.0M to $9.0M**
System Options	
Option 1 – Ground Processor (Workstation Based)	$1.4M to $1.8M
Option 2 – Airborne Realtime Image Display (Note: multiply this by two for real-time interferometry)	$500K to $750K

Annual maintenance & repair costs for airborne INSAR systems are estimated to be in the range of $250K to $500K. Operational costs for INSAR systems vary widely based on the amount of utilization, but are generally in the range of $500-1500 per data collection hour including a single-operator and all expendables/consumables. These costs do not include the costs of operating and maintaining the host aircraft.

Delivery schedules for INSAR systems are on the order of 12-24 months based on supplier scheduling and aircraft availability.